Warsaw University of Life Sciences - SGGW
Faculty of Forestry

Eberswalde University for Sustainable Development – HNEE Applied University
Faculty of Forest and Environment

Lea Henning
SGGW Student ID 158513
HNEE Student ID 520721

Early Recognition of Changes in the Health Status of Norway Spruce with Hyperspectral Data

Master thesis
Forest Information Technology

Thesis supervised by

Dr. rer. nat. Nicole Pinnel
DFD – German Remote Sensing Data Centre
DLR – German Aerospace Centre

Prof. Dr. Jan-Peter Mund
Faculty of Forest and Environment
Eberswalde University for Sustainable Development (HNEE)
University of Applied Sciences

Warsaw, Eberswalde, 2014

Oświadczenie promotora pracy

Oświadczam, że niniejsza praca została przygotowana pod moim kierunkiem i stwierdzam, że spełnia ona warunki do przedstawienia jej w postępowaniu o nadanie tytułu zawodowego.

Tutor's Declaration

I declare, that the diploma thesis was prepared under my supervision and I state it fulfils the conditions for present it in the professional title proceedings.

Erklärung des Betreuers

Ich erkläre, dass die vorliegende Arbeit durch mich betreut wurde und die Voraussetzungen für die Durchführung eines Master-Verfahrens erfüllt.

Data	Podpis promotora pracy .....
Date	*Tutor's signature*
Datum	*Unterschrift des Betreuers*

Oświadczenie autora pracy

Świadom odpowiedzialności prawnej oświadczam, że niniejsza praca dyplomowa została napisana przeze mnie samodzielnie i nie zawiera treści uzyskanych w sposób niezgodny z obowiązującymi przepisami.

Oświadczam również, że przedstawiona praca nie była wcześniej przedmiotem procedur związanych z uzyskaniem tytułu zawodowego w wyższej uczelni.

Oświadczam ponadto, że niniejsza wersja pracy jest identyczna z załączoną wersją elektroniczną.

The author's declaration

Being aware of legal liability I declare, that the Master thesis was written by myself and it does not include any contents obtained in the illegal way.

I also declare that the presented thesis was not a subject of any university professional title's proceedings previously.

In addition I declare, that the presented version of the thesis is identical with the electronic version included.

Erklärung des Verfassers

Ich versichere, dass die vorliegende Arbeit durch mich angefertigt wurde und kein unrechtmäßig erworbenes Material enthält. Über die Konsequenzen einer Verletzung dieses Grundsatzes bin ich mir bewusst.

Ich versichere weiterhin, dass die vorliegende Arbeit zuvor keiner anderen Universität zur Erlangung eines wissenschaftlichen Grades vorgelegt wurde.

Zusätzlich erkläre ich, dass die schriftliche Fassung dieser Arbeit mit der beigefügten digitalen Fassung übereinstimmt.

Data	Podpis autora pracy .....
Date	*The author's signature*
Datum	*Unterschrift des Verfassers*

Streszczenie

Wczesna identyfikacja zmian w zdrowotności Świerka pospolitego (*Picea abies L.*) za pomocą danych hiperspektralnych.

Ostatnie badania pokazały, że monokultury Świerka pospolitego (*Picea abies L.*) są wrażliwe na zmiany klimatu (Bawarski Państwowy Instytut Leśnictwa (LWF), 2009) i dodatkowo podatne na różne zagrożenia takie jak silny wiatr lub gradacje szkodników. Szczególnie w związku z ostatnim, wczesne rozpoznanie zmian w stanie zdrowotności może pomóc w minimalizowaniu strat pod względem ekonomicznym.

Fundamentalnym pomysłem wykorzystanym do analizy spektralnego odbicia igieł Świerka pospolitego jest to, że w przeciągu pięciu miesięcy po sztucznym osłabieniu drzew, zakres spektralnego odbicia igieł wykazuje różnice, które mogą umożliwić rozróżnienie drzew osłabionych od drzew kontrolnych. Sztuczne osłabienie drzew poprzez obrączkowanie prowadzi do szerokiej w czasie detekcji zmian w związku z powolnym zamieraniem drzew.

Czas, w którym igły ciągle są zazielenione, a zmiany w odbiciu spektralnym świadczą o spadku kondycji zdrowotnej drzew zaobrączkowanych jest najbardziej interesujący. Podczas trwania badań igły były pobrane prosto z koron drzew, zaś odbicie spektralne było mierzone w laboratorium.

Porównanie zakresu spektrum pomiędzy obiema grupami zostało przeprowadzone za pomocą analizy głównych składowych (PCA), odległością Jeffries-Matusita i różnymi wskaźnikami związanymi ze zdrowotnością roślinności.

Wyniki pokazały, że nie jest możliwym rozróżnienie drzew zaobrączkowanych i drzew kontrolnych zastosowanymi metodami po pięciomiesięcznym okresie czasu. Niniejsza praca magisterska ukazuje drzewa jako złożone systemy w związku ze sposobem transportowania wody i asymilatów. Rozpiętość czasu od „uszkodzenia" do „symptomu" zależy od różnorakich czynników. To powoduje, że „wczesne" rozpoznawanie problemów zdrowotnych bazując na odbiciu spektralnym igieł jest trudnym w przypadku drzewostanów.

Abstract

Early Recognition of Changes in the Health Status of Norway Spruce with Hyperspectral Data

Recent studies show that Norway spruce monocultures are fragile with regard to climate changes (Bayerische Landesanstalt für Wald und Forstwirtschaft (LWF), 2009) and furthermore vulnerable to different threats like storm damages or insect infestations. Especially due to the last mentioned, early detection of changes in the health status could help minimizing economical loss.

The fundamental idea which lead to Norway spruce needle reflectance spectra analysis is, that within a time period of five months after artificial weakening of trees, reflectance spectra of needles show differences, which might make it possible to distinguish between weakened and control trees. Artificial weakening through ring-barking leads to a wide time frame for change detection due to a slow die back of trees.

The point of time where needles still appear green but changes in reflectance spectra indicate a decline in the health status of ring-barked trees is of special interest. During the whole period needles were sampled directly within tree crowns and reflectance spectra were measured in a spectral laboratory.

Comparison of spectra between both groups was conducted with the principal component analysis, the Jeffries-Matusita Distance and different health related indices.

The results show that it is not possible to distinguish between ring-barked and control trees with the applied methods after a period of five months. This thesis illustrates that trees are complex systems with regard to their water- and assimilate transportation system. Time span from 'damage' to 'symptom' is dependent on various different factors. This makes 'early' recognition of health problems with needle reflectance spectra difficult in forest stands.

Zusammenfassung

Früherkennung von Gesundheitsveränderungen in Fichtenbeständen mit Hyperspektralen Daten

Im Hinblick auf den Klimawandel und damit verbundenen, zunehmenden Schadereignissen wie Sturmschäden oder Insekten Kalamitäten, haben sich Fichtenmonokulturen als besonders anfällig erwiesen (Bayerische Landesanstalt für Wald und Forstwirtschaft (LWF), 2009). Frühzeitiges erkennen von Veränderungen im Gesundheitszustand von Wäldern kann dabei helfen, größere ökonimische Schäden zu vermeiden.

Die grundlegende Idee dieser Arbeit ist, durch künstliche Schwächung von Fichten Veränderungen in den Nadeln hervorzurufen. Die künstliche Schwächung erfolgt hierbei durch ringeln. Innerhalb von 5 Monaten nach der Ringelung werden kontinuierlich Nadelproben genommen und die Reflekionsspektren im Labor gemessen. Festzustellen gilt er hierbei, wann und wie sich die Schwächung im Reflektionsspektrum der Nadeln zeigt. Die Ringelung ermöglicht hierbei eine langsame Schwächung der Bäume.

Von besonderem Interesse ist der Zeitpunkt an welchem die Nadeln noch grün erscheinen, sich jedoch ein veränderter Gesundheitszustand bereits im Reflektionsspektrum zeigt. Die Nadeln werden direkt aus der Krone entnommen, die Nadelspektren zeitnah im Labor gemessen.

Ein Vergleich zwischen den Reflektionspektren der geringelten und der kontroll Gruppe wurde mit der Hauptkomponentenanalyse, dem Distanzmaß nach Jeffries-Matusita und verschiedenen Indizes durchgeführt, welche direkt mit dem Gesundheitszustand von Vegetation in Verbindung gebracht wurden.

Die Ergebnisse zeigen, dass es nach fünf Monaten, mit der angewendeten Methodik, nicht möglich ist, zwischen den geringelten und den kontroll Bäumen zu unterscheiden. Im Bezug auf ihr Wasser- und Assimilat Transportsystem sind Bäume sehr komplexe Systeme. Der Zeitraum von der Schädigung hin zu sichtbaren Symptomen hängt von manigfaltigen Faktoren ab, welche mit einbezogen werden müssen. All das macht Früherkennung von Änderungen im Gesundzeitszustand von Wäldern mit der Hilfe von Reflektionsspektren kompliziert.

Contents

List of Tables

List of Figures

Nomenclature

AVHRR	Advanced Very High Resolution Radiometer
BaySF	Bavarian State Forest
BH	Bhattacharyya Distance
BOKU	University of Natural Resources and Life Sciences in Vienna
DLR	German Aerospace Centre
EVI	Enhanced Vegetation Index
EWT	Equivalent Water Thickness
GIMMS	Global Inventory Modelling and Mapping Studies
ISLSCP	International Satellite Land Surface Climatology Project
JM	Jeffires-Matusita Distance
LAI	Leaf Area Index
LWF	Bayerische Landesanstalt für Wald und Forstwirtschaft
NASA	National Aeronautics and Space Administration
NDII	Normalized Difference Infrared Index
NDLI	Normalized Difference Lignin Index
NDVI	Normalized Difference Vegetation Index
NDWI	Normalized Difference Water Index
NIR	Near Infrared
PCA	Principal Component Analysis
PNV	Potential Natural Vegetation
PSRI	Plant Senescence Reflectance Index
RENDVI	Red-Edge Normalized Difference Vegetation Index
SIPI	Structure Insensitive Pigment Index
SWIR	Short Wave Infrared
VWC	Vegetation Water Cnntent

1. Introduction and Objective

Forests all over the world are subject to a variety of disturbances e.g. species invasion, insect plagues and disease outbreaks or climatic events like hurricanes, drought, fire or floods. All these events have an influence on ecosystem functions, structure and species composition of a forest ecosystem and can have damaging impacts, to the point of complete destruction of whole areas (Boa, 2003). As a result of climate change, it is expected that frequency, duration intensity of disturbances will increase, as well as forests' susceptibility. Additionally, interactions between the above mentioned events make prediction of their impact on future forest disturbances more difficult (Food and Agriculture Organization of the United States, 2010). In context with climate change and increasing threats the terms 'vitality' and 'health' are often used to describe the condition of forests. They are often used synonymously, whereas it can be useful to distinguish between these words.

The term vitality derives from the Latin word *Vita*, which means life and life force. In forestry it implies the ability of a tree or a forest stand to survive and adapt under given environmental circumstances (Shigo, 1994). O'Laughlin *et al.* (1994) wrote that forest health is a condition of forest ecosystems that sustains their complexity while providing for human needs. Furthermore Helms (1998) described forest health as the perceived condition of a forest derived from concerns about such factors as age structure, composition, function, vigor, presence of unusual levels of insects or diseases and resilience to disturbance. Based on these definitions it makes sense to distinguish between vitality, the ability to survive and adapt, and health, the actual condition of a tree or forest stand. The example, that a tree might be ill but due to its good vitality it is able to persist while another tree, which is not vital would not, illustrates the difference between 'vitality' and 'health'. For a whole forest stand vitality means that it could regenerate and overcome damages or injuring accidents on its own, without being affected in its survivability.

According to the definitions described before, vitality is a competence and not a condition. It can not be directly measured. Therefore it seems obvious to measure the health status of forest stands or trees. It can be described qualitatively by specifying symptoms or damage and quantitatively through assessments of crown conditions (Boa, 2003). Doing so it is challenging to define at which point a tree is healthy or unhealthy. Additionally it is important to keep in mind that observations concerning the health status always have to be evaluated relative to other stands or trees of the same species within the same development phase and place of location (Klug, 2005).

In Germany an observed decline of forest during the early 70's led to risen awareness about forest functions and together with pressure on politics it resulted in the Federal Forest Act in 1975. Among others it includes measures concerning the treatment of forest and a detailed forest inventory which has to be implemented every 10 years (Bundesministerium für Ernährung, 2011). This thesis focuses on Bavarian forests, where spruce monocultures are the dominant forest type (Bundesministerium für Ernährung, 2004). Besides wood production forests fulfill additional functions like CO_2 binding and groundwater protection. Within these forest stands vitality plays a special role because monocultures are generally regarded to be more vulnerable to massive damages due to insect infestations or storm damage. Conventionally forest health is determined for the annual forest status report and the forest inventory with data about crown conditions (Bundesministerium für Ernährung, 2012). From these data the health status of a tree can be deduced with factors such as greenness and size of leaves as well as foliation. Collecting these field data is an extensive and time consuming procedure.

At this point remote sensing offers a good possibility for data collection. In times of changing climate and increasing interest in nature conservation and wood as energy resource and building material it is important to monitor forests and their behavior under changing environmental circumstances at a large scale. This is because health is directly linked to functionality of forests as ecosystems, CO_2 deposits and their productivity. Many different remote sensing techniques were developed to measure health related aspects like water-, nitrogen- and chlorophyll contents of canopies or foliation. Remote sensing can help to describe how forest cover changed over time and to interpret changing processes at large and small scales. Furthermore, it can help to detect damage contemporarily which is helpful, for example in case of insect infestations which can threaten whole forest stands and call for timely countermeasures. Finally, early detection implemented in the forest itself or by remote sensing techniques, is the basis for an effective management of tree or forest health problems.

In case of Norway spruce monocultures in Bavaria, where insect calamities lead to considerable damages in forest stands, an early detection of a decrease in the health status could help minimizing biological and economical impact. Therefore the German Aerospace Centre (DLR), the University of Natural Resources and Life Sciences in Vienna (BOKU), the Bavarian regional office for Wood and Forestry (LWF) joined up for the VitTree project. The aim of this project is the early detection of stress in forests. This master thesis is part of VitTree and evaluates the

reflectance data of Norway spruce needles recorded in the spectral laboratory as a basis for change detection with HySpex airborne data.

As of now it is possible to detect damaged trees and to derive health linked aspects of trees with remote sensing techniques. Nevertheless it is still necessary to determine at which point of health deterioration it is possible to distinguish between healthy trees and trees with reduced healthiness. Research in this field is ongoing and this question was central in this thesis.

THE OBJECTIVE is to determine the earliest date where it is possible to detect changes within the reflectance spectrum of *Picea abies* needles after damage, which is fatal in the long term.

HYPOTHESIS 1 It is possible to distinguish optically between healthy and damaged trees after a time period of five months.

HYPOTHESIS 2 It is possible to define a moment at which needles appear green but a change within the sampled reflectance spectra suggests a decrease in the health status of a tree.

HYPOTHESIS 3 It is possible to detect these changes with statistical methods like the principal component analysis or mean comparison of indices.

2. Concept and Idea

This master-thesis is part of the project VitTree which is conducted in cooperation between the the Bavarian regional office for Wood and Forestry (LWF), the Bavarian State-forest (BaySF), the German Aerospace Centre (DLR) and the University of Natural Resources and Life Sciences in Vienna (BOKU). Aim of the project is the early detection of changes in spectral signatures of forest stands due to degradation, preferably before any visible changes in needle color can be detected in the field. For this purpose artificial weakening of Norway spruce trees was carried out, simulating the effect of bark beetle attacks, in the forest district 'Wasserburg am Inn'. The idea is to achieve weakening through ring-barking, which is ultimately lethal but only in the intermediate term. Primary effect of ring-barking is that the trees are stressed and therefore show stress symptoms in the needle reflectance spectra.

Ring-barking or girdling means causing an interruption of assimilate transportation to the root system of a tree. For this purpose a circumferential strip of bark, including cambium and phloem, sometimes also parts of the xylem, is removed (Roth *et al.*, 2001). This method can be used in forest stands where utilization of wood is not of economic interest (small tree diameters, low wood quality, difficulty of access) or harvesting would lead to excessive damages within the stand. It also can be an alternative to mechanical felling of competitive trees (Roth *et al.*, 2001). An advantage of this method is that ring-barked trees remain in the stand for shadowing younger trees and understorey while maintaining stability of the stand. Furthermore it is not necessary to remove these trees mechanically, which saves costs. As mentioned by Roth *et al.* (2001) a risk is that ring-barked trees fall down uncontrolled. As ring-barking is a severe and irreversible intervention in the trees water and assimilate transportation system it will lead to a decease of the ring-barked trees. Experiences show that a decease of affected trees can be expected after between one and three, sometimes up to four years (Roth *et al.*, 2001). For this project a bark-strip of 15 to 20 cm width was completely removed leaving the xylem intact.

Two sample plots (see fig. 4.1) were chosen in the study area described in chapter 4. Per sample plot 70 trees were ring-barked in the mid of June (13.and 14.06.2013). Beside the weakened trees, 70 control trees were marked. For visualization and identification on aerial imagery GPS coordinates of each tree were recorded. Ring-barked trees were inspected weekly for monitoring of crown condition and bark beetle attacks to remove affected trees contemporarily.

To gather airborne hyperspectral data for evaluation of forest health in the study area, a flight campaign was planned with one overflight before ring-barking (between

13.05.2013 and 31.05.2013) and continuous overflights for a time line, beginning from the 1st of July 2013 until 31st of August 2013. Furthermore ground reference data were sampled four times by taking needle twigs directly from tree crowns in July (18.07.2013), August (20.08.2013), September (10.09.2013) and November (20.11.2013). Needle reflectance spectra measurements took place in the DLR spectral laboratory (described in chapter 4).

Figure 2.1.: Ring-barking of trees (photos: M. Immitzer)

3. Basics and State of The Art

In this chapter an introduction of the investigated tree species as well as a description of the water- and assimilate transportation system in trees are given. It also includes a short introduction to spectroscopy and closes with a literature review about vegetation monitoring and forest health detection in remote sensing.

3.1. Norway spruce

Naturally Norway spruce grows in Europe within subalpin altitudinal zones where the vegetation period is too short for beech or fir trees. Beyond this range of distribution, natural occurrence is limited to particular sites on which exceptional spruce stands occur. An example are spruce-chalk forests with large duff accumulation within cold air leading boulder-humus-mosaics (Bayerische Landesanstalt für Wald und Forstwirtschaft (LWF), 2009). Concerning water supply Norway spruce is a demanding tree. It requires medium up to fresh soils without stagnant moisture. However nutrient requirements are modest. Figure 3.1 visualizes the potential natural vegetation (PNV) of Norway spruce in Bavaria (Bayerisches Landesamt für Umwelt, 2014). It can be noticed that naturally occurrence of Norway spruce in Bavaria is limited to the very southern part and some small areas in western and north-west Bavaria.

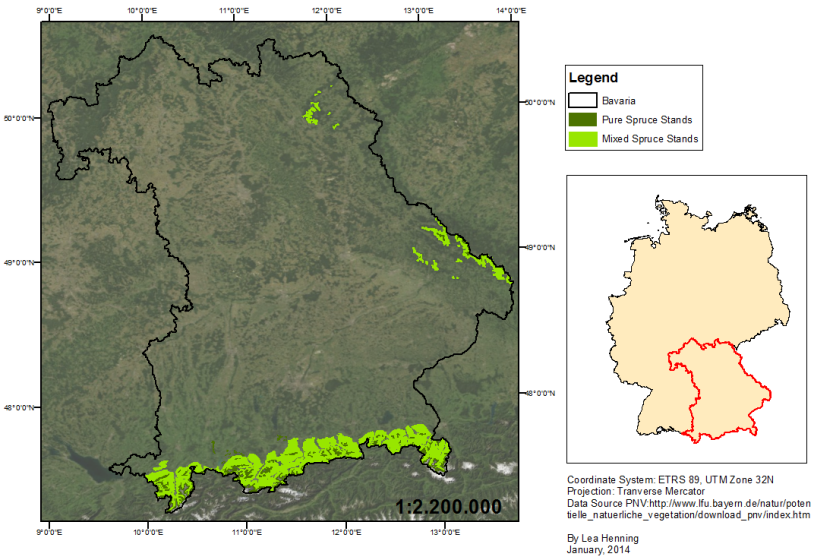

Figure 3.1.: Potential Natural Vegetation of Norway Spruce in Bavaria

Broad representation of Norway spruce in Bavarian forests is rooted in history. Increasing population and intensive usage of forests in Germany during the 18th

century lead to a timber shortage. Timber extraction for increased construction or military activities, overgrazing and browsing by increased game population lead to numerous barren areas. Realization of decreasing forest areas lead to fear of timber shortage and to sustainable management of the remaining forests. Furthermore reforestation of depleted areas was propagated. Due to their straight growing trunk and fast growing characteristics spruce and pine trees were promoted. Beneficial for spruce growth was removal of biomass (litter for barns or fuel-wood) of the forest which lead to depleted soils and with that to unfavorable growing conditions for other tree species and reduces palatability to game. Expansion of Norway spruce was already in progress when coniferous monocultures became wide spread at the beginning of the 19th century (Freitag, 2013). Although coniferous monocultures met the needs of rapidly growing industries and cities, they always were ecologically unstable. Insect infestations at large scale as well as storm damages wreak havoc until today. This impacts wood production as well as additional forest functions like regulation of water supply, binding of carbon dioxide, filtering of air pollutants and usage as recreational area (Freitag, 2013).

During the 80s a rise in forest decline lead to increased public interest. It was topic in the media for years, many different opinions on causes and remedies were discussed and it became a political theme (Schäfer, 2001). Certainly the forest decline lead to a rethinking of environmental threats that forests are exposed to. Result of this debate were regulations for air-quality improvement and methods for forest conversion from monocultures to mixed forests.

In Bavaria around half of the forests are pure Norway spruce stands (Bundesministerium für Ernährung, 2004) which makes it the most important tree species. Although forest conversion from monocultures to mixed stands, which are more resistant against insect calamities or storm damages, is in progress Norway spruce will remain one of the main trees species in these forest stands. Due to unfavorable site conditions it will still be vulnerable against insect calamities and storm damages. This leads to the concern to monitor spruce stand and detect changes in the health status which may be important signals related to storm damages or insect infestations.

3.2. Plant physiology

For better understanding of hyperspectral measurements of health in spruce stands it is necessary to know some basics about Norway spruce, plant physiology and stress symptoms of trees. This chapter describes basic facts about water and assimilates cycles in trees as well as stress symptoms.

3.2.1. Water and assimilate transportation in trees

The principle behind the experiment which yields the data that is analyzed in this thesis, as described in chapter 2 is based on biological mechanisms of water and assimilate transportation within the tree. Growth efficiency is predominantly dependent on water supply and temperatures. The influence of temperatures will be excluded from this experiment as they constrain growth beyond the vegetation period. Within the vegetation period often the amount of accessible water determines stand conditions. As a dissolvent it facilitates transportation of substances within plants as well as the exchange in between plants and the atmosphere. Furthermore it serves as a cooling system and protects needles and leaves from overheating. Finally water is required for photosynthesis. To ensure supply of water within the whole tree an efficient water-transportation system is essential (Raven *et al.*, 2006). This is sustained within trees with the vascular tissue consisting of xylem and phloem. Mostly xylem is described as 'the water transportation system' while phloem serves as 'the assimilate transportation system'. Last-mentioned transports the assimilates from sources, which are mainly leaves where the photosynthesis takes place, to sinks, which are places where they will be stored or consumed (Raven *et al.*, 2006).

Figure 3.2 gives a simplified overview about the water- and assimilate transportation dynamics. The driving force for this system is transpiration, which is the process of losing water through leaves, bark and other parts of the plant body. Water loss through leaves creates a negative pressure gradient which leads to a suction of water upwards. Most of transpiration is controlled by orifices in the leaf surface called stomata, which are responsible for around 90% of water loss due to transpiration (Raven *et al.*, 2006). Furthermore these cells offer the entry for carbon dioxide which is needed for photosynthesis. Further detail can be found in 'Biologie der Pflanzen' by Raven *et al.* (2006).

In answer to a negative pressure gradient within the water-transportation system the root system takes up water and dissolved minerals from the soil. This aqueous solution is transported in the xylem to leaves where it is used for photosynthesis or alternatively to buds and fruits. During the process of photosynthesis assimilates are produced which are transported into the phloem and to the root system or to buds and fruits. In doing so leaves from the upper part of trees provide assimilates for mainly fruits, buds and new leaves while assimilates produced by lower levels in the crown are mainly transported to the root system (Raven *et al.*, 2006).

Figure 3.3 shows a cross section through the described transport tissue, here in an old linden tree trunk where the basic principle of cambium, xylem and phloem

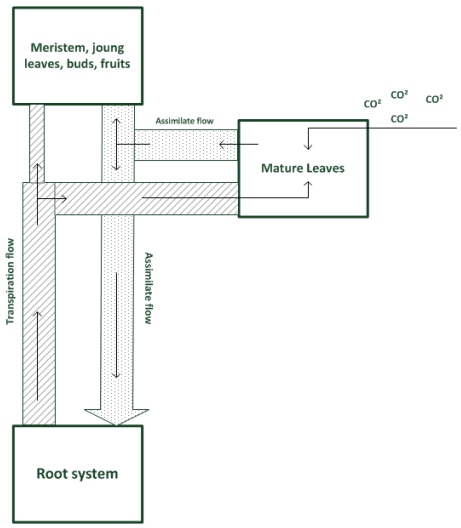

Figure 3.2.: Circulation of water and assimilates in plants according to Pate (1975)

creation is the same. The cambium, a thin layer of living cells between sapwood and bark, produces xylem cells on the inner and phloem cells on the outer side (Raven *et al.*, 2006). It is also responsible for tree rings as its growth varies over the course of the year. In spring it produces earlywood, which is of lower density than latewood, with relatively large, thin-walled cells. In comparison, latewood has smaller cells with thicker cell walls and is produced in late summer until autumn (Raven *et al.*, 2006). The pass from earlywood to latewood might be gradual and not easy to notice. As already mentioned, xylem is mainly responsible for water and nutrient transportation up to the crown and due to its lignification also for stability. The transportation takes place in a number of recently built year rings, depending on the tree species (Shigo, 1994). At the same time in which the cambium produces xylem cells it also produces phloem cells as well, although in a lesser number. As mentioned before, phloem is mainly responsible for assimilate transportation from sources to sinks (Raven *et al.*, 2006).

This transportation cycle is directly connected with vegetation cycles of trees. These consists of a growing season, which in temperate zones is limited by temperature and dormancy, when growth of leaves, bark and wood is halted. Within the growing season different growing cycles can be observed, concerning root and shoot growth of a tree. Normally root and shoot growth alternate each other and vary typal. Here the case for Norway spruce will be shown: Usually root growth of Norway spruce initiates in spring before bud burst with incipient melt water (Resa, 1877). It hast its first maximum from March until April (Resa, 1877). This comes along with intense usage of embedded carbohydrates (Raven *et al.*, 2006). Once sprouts start showing up, mainly around April, root-growth decreases while sprout growth increases. This

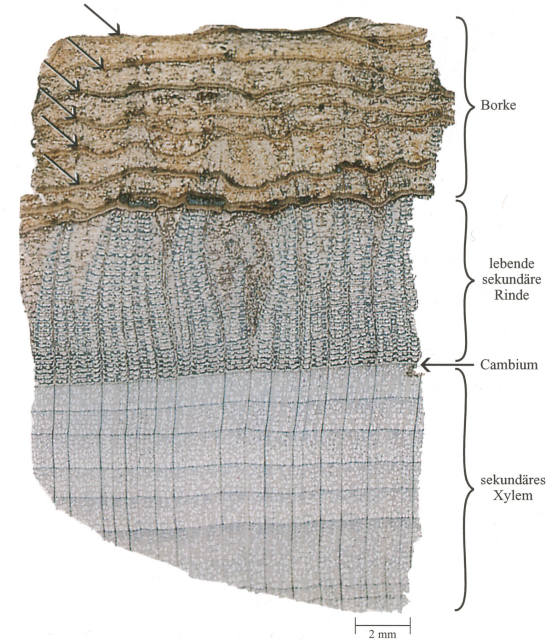

Figure 3.3: Cross section through bark, secondary bark and parts of secondary xylem of an old Tilia americana trunk. Different layers of bark are visible (bolts). Between it and the cambium, living secondary bark is located, which can be clearly differentiated from secondary xylem (Raven et al.*, 2006).*

in turn leads to an increased carbohydrate and water demand in the crown (Raven *et al.*, 2006). A second intensified root growth can be observed again in autumn when sprout growth stops and rainy weather becomes more frequent (Puhe, 2003) between September and October (Resa, 1877). Root growth depends completely on carbohydrate supply from the sprouts, while sprouts need water with minerals and nutrients from the root system (Lösch, 2003).

Summing up: The vegetation cycle comprises of growing season and dormancy. During the growing season alternating growth of roots and shoots occurs. Due to these interconnected cycles, the direction of transportation of assimilates underlies changes.

3.2.2. Stress symptoms of vegetation

Some examples for stress are listed in Lichtenthaler (1996): heat, water shortage, natural mineral deficit, insects infestations, long rain periods, air pollutants, acid rain or surplus of ammonium. Responses to these stress factors can be specific and unspecific (Beck *et al.*, 2007) as well as they can cause economical and ecological loss. Generally stress can be described as a state of strain of an organism. As long as the effects of a stress factor are not irreversible, trees react with physiological, morphological and biochemical adaption which increases resistance against the present stress factor (Vollenweider & Günthardt-Goerg, 2005).

If a certain threshold of stress is exceeded and damages change from reversible to irreversible parts or whole plants die off (Larcher, 2001). As mentioned before,

adaptability is closely connected with stress. It can be described as the ability of plants to reorient themselves when they are outside of optimal environmental conditions. This is only possible within a certain range which is defined by minimum and maximum resistance (Lichtenthaler, 1996). Furthermore it should be noted that stress can be categorized into short- and longterm stress (Lichtenthaler, 1996), which have different effects of varying importance. As stress is a routine event and the effects are dose-dependent (Lichtenthaler, 1996) it is interesting to find out at which point the tolerance limit is exceeded. Generally it can be noted that initially stress leads to growth reduction, interference in reproduction capacity or decreased resistance against parasites before it might become fatal. Trees do not have many possibilities to respond to stress and not every stress factor has its characteristic symptom. There are few significant symptoms for many single or combinations of stress factors.

For detection of stressed vegetation, respectively forest in this case, the range of adaptation capacity is of high importance. The difference to normal state and the duration of a stress situation needs to be examined. However, with regard to water or nutrient supply, species respond very differently (Zang *et al.*, 2011). While looking for stress in trees, one should keep in mind that under stress two inverse reactions, stabilization and destabilization, occur (Larcher, 1987). At best both hold balance and a new normal state can be reached. It is important to mention that stress is a routine event which is necessary for evolution.

For a simplified overview about stress and to determine at which point it becomes dangerous for plants generally, Lichtenthaler (1996) developed the 'Stress Concept' which consists of three stages:

The alarm reaction shows a deviation of normal conditions with beginning decline of vitality.
The resistance phase follows and includes the adaptation during continuing stress from stressed to normal status.
The stage of exhaustion is reached if stress persists too long and adaptation is no longer possible. In this stage, too high stress intensities lead to over-strain of the adaptation capacity.

In conclusion: Water has a widespread importance in many plant physiological processes and exchange procedures between the plant itself and its environment. Due to this a spill-over or deficit in water supply can determine the conditions of survival. Stress is not an exceptional circumstance, it is necessary for adaptation of

vegetation to new environmental circumstances and only risky if a certain threshold is exceeded. Definition of this threshold is always challenging.

3.3. Remote sensing of vegetation

The term remote sensing means the determination of object characteristics from longer distances. Measuring fluorescence, reflectance of incoming and emission of thermally produced electromagnetic radiation in the spectral range between microwaves and ultraviolet, allows derivation of changes in vegetation cover, state of health and productivity (Buschmann, 1993). In case of areas which are not easy to access, remote sensing offers a good possibility to monitor changes in vegetation covers as for example forest clearance in the rainforest or permafrost melting in the west Siberian plain. Due to different spatial and spectral resolutions of the available sensors it is not always possible to fulfill each requirement and a compromise needs to be found between needs and available data. Additionally it is helpful to have ground truth data for verification of remotely sensed data. For this thesis hyperspectral ground truth data were analyzed for later comparison with hyperspectral airborne data. As very subtle changes are expected, reflectance spectra were firstly measured in the laboratory to avoid atmospheric impacts. Analysis of these data works in the same way as analysis of hyperspectral airborne data with which these changes should be observed later. In this section a short introduction about spectroscopy is given and afterwards a literature review gives an overview about methods, indices and wavelengths related to vegetation and forest health.

3.3.1. Spectroscopy

The word spectrum is based on the Latin expression for 'image' or 'phenomenon' (lat. *spectrum*). Generally used to express variability, in this thesis it it describes a range of electromagnetic radiation. Besides light, this includes other radiation like microwaves, thermal- and x-radiation. The range of visible light which is detectable by the human eye is only a small portion of the wavelength spectrum (fig. 3.4). With technical support it is however possible to detect radiation beyond the visible range of light and produce 'images' with more information. It is like a fingerprint for surfaces and with it, different surfaces or materials can be distinguished.

Spectroscopy is applied for remote sensing with hyperspectral sensors. The difference between multi- and hyperspectral data is that in case of hyperspectral data a quasi-continuous spectrum is produced with way more and more narrowly-spaced bands than with multispectral sensors (see fig. 3.6).

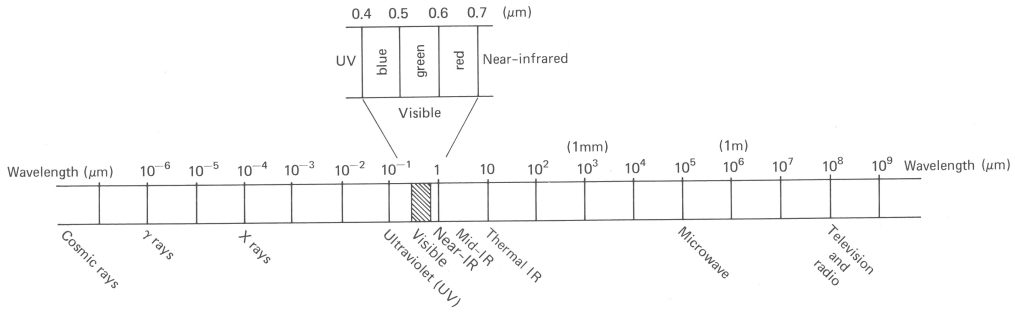

Figure 3.4.: The electromagnetic spectrum (Lillesand et al.*, 2004)*

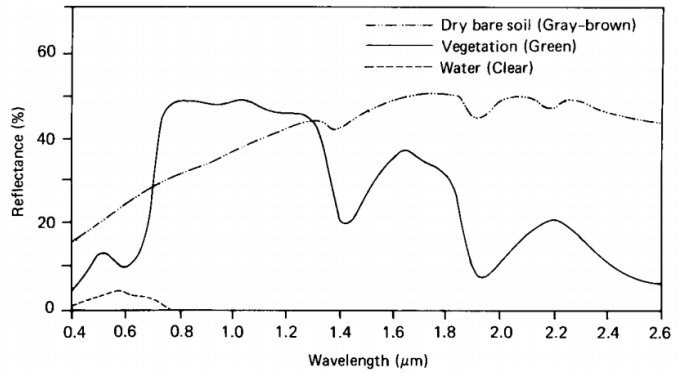

Figure 3.5.: Typical spectral reflectance curves for water, vegetation and soil (Lillesand et al.*, 2004)*

Assuming a healthy, green forest the spectrum is a typical vegetation spectrum (see fig. 3.7) with relatively low reflectance between 400 to 500 nm (blue light) and 600 to 700 nm (red light) while the green portion (around 500 to 600 nm) is reflected (green peak). Vegetation reflectance increases remarkably between red and near infrared (700 to 1000 nm), which is called 'red-edge' (Mohammed *et al.*, 2000). This typical reflectance spectrum of green, healthy vegetation originates in photosynthetic activities of green leaves and their reflectance, respectively transmittance, characteristics. Especially in broadleaved forests, seasonal changes are important to consider. Detailed information about the background of vegetation reflectance characteristics were described by Jones & Vaughan (2010).

3.3.2. Literature review

Based on the the spectrum of vegetation and its changes a lot of research concerning forest health status changes has been done. Gitelson (2012) summarized that three basic approaches for estimating the green vegetation fraction from remotely sensed data exist: neural networks, spectral mixture analysis and vegetation indices. Commonly used for proximal sensing are vegetation indices (Gitelson, 2012).

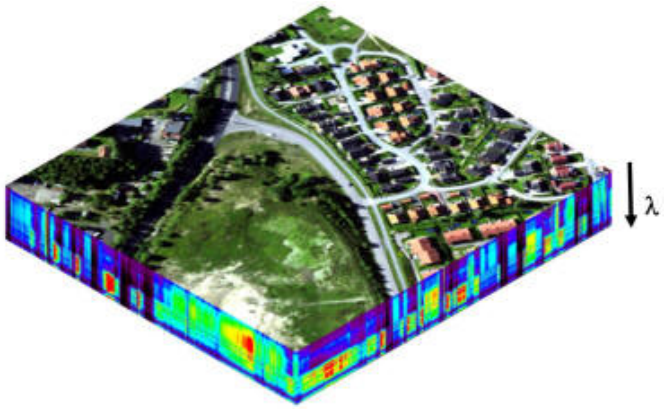

Figure 3.6.: Hyperspectral data cube with λ as wavelength (Norsk Elektronik Optikk, 2013)

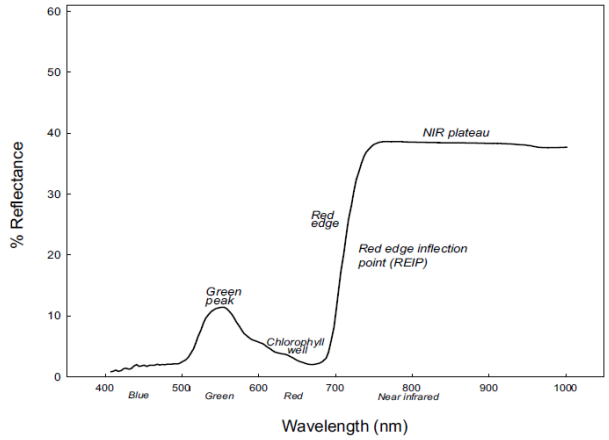

Figure 3.7.: Typical vegetation reflectance curve by Mohammed et al. *(2000)*

Photosynthetic activity Maybe the most significant characteristic, found in a vegetation spectrum, is the red-edge. Clark *et al.* (1993) described the edge along the red/infrared boundary which is sharp and steep in green and healthy vegetation. As vegetation becomes stressed or senescent, the red-edge shifts towards shorter wavelengths and the width of the absorption band decreases. This difference between the reflectance minimum in the visible red region and reflectance maximum in the near-infrared region primarily shows the photosynthetic activity (Clark *et al.*, 1993) and consequently if vegetation is alive. One of the commonly used red-edge indices is the Normalized Difference Vegetation Index (NDVI) (Rautiainen, 2005). It is a normalized ratio index which simply requires reflectance data in the red and the near-infrared portion of the electromagnetic spectrum.

One example for using the NDVI is the Global Inventory Modelling and Mapping Studies (GIMMS). It is a global measure of NDVI and covers a 22-year period. The dataset is derived from the Advanced Very High Resolution Radiometer (AVHRR)

with a spatial resolution of 1 km. It was originally generated to characterize biophysical change which was defined in the International Satellite Land Surface Climatology Project (ISLSCP) Initiative II collection. Available are two values per month, the maximum NDVI value for the first fifteen days of the month and the maximum value for the remaining days. It is corrected for calibration, volcanic aerosols, view geometry and other effects not related to vegetation change (National Aeronautics and Space Administration (NASA), 2014). With this dataset it is possible to detect post-fire vegetation trends (Yi *et al.*, 2013), global trends in seasonality (Eastman *et al.*, 2013) or variability in the net primary production of vegetation (Zhang *et al.*, 2014). These measurements are relatively rough due to the low spatial resolution of the GIMMS dataset but nevertheless linked to the health status of vegetation. With changed and improved spectral resolutions of the available data, the NDVI was modified. There are for example the 'red-edge spectral index' (Delegido *et al.*, 2013) and the ND_{680} (Sims & Gamon, 2002). The hyperspectral variant, ND_{680}, was introduced because differentiation within the red and near-infrared range became possible thus a wider range of bands was available. On the other hand different studies (Jackson, 2004; Rautiainen, 2005; Sellers, 1985; Chen & Cihlar, 1996) showed that NDVI tends to saturate and changes in chlorophyll activity are hardly detectable. The 'red-edge spectral index' was reported not to saturate like the NDVI (Delegido *et al.*, 2013) which is an advantage for differentiation within closed vegetation or forest covers. Another often used red-edge vegetation index which is also reported to be more sensitive to moderate-to-high vegetation biomass is the Enhanced Vegetation Index (EVI) introduced by Huete *et al.* (1997).

Vegetation water content The NDVI was not only used for measurements of photosynthetic activity. Jackson (2004) reported that the NDVI can also be used for derivation of vegetation water content (VWC), although it is limited to specific regions and needs to be supported with ground truth data. In contrast to the NDVI the Normalized Difference Water Index (NDWI) was especially designed for measuring canopy water contents. It was described by Gao (1996) and has both bands in the high reflectance plateau (0.86 μm and 1.24 μm). It is sensitive to changes in liquid water content of vegetation due to canopy scattering which enhances water absorption (Gao, 1996). Furthermore, Gao (1996) described that the NDWI increases with increasing leaf layer. Based on SPOT-VEGETATION data, this index shows uncertainties in remote sensing of water content at canopy level because the short wave infrared (SWIR) channel was questionable to estimate VWC (Ceccato *et al.*, 2002a,b). These uncertainties are supported by Hunt & Yilmaz (2007). Detection of incipient stages of water stress in plants might not be detectable in SWIR reflectance

(Hunt & Yilmaz, 2007). They investigated an alternative method to the NDWI: The Normalized Difference Infrared Index (NDII) (Hunt & Yilmaz, 2007). This index includes reflectance at near-infrared (NIR) and SWIR bands. It estimates the amount of SWIR radiation which is absorbed by liquid water in foliage. This index also makes it possible to derive changes larger than 0.5 m^2 in the leaf area index (LAI) if leaf equivalent water thickness (EWT) is constant (Hunt & Yilmaz, 2007). The LAI is a dimensionless variable which is defined as half of total green leaf area per unit of ground (Chen & Black, 1992) which can be used characterize changes in vegetation since it responds rapidly to changes in vegetation behavior citepRautiainen2005. It was noted that in the NDII saturation shows up as well (Hunt & Yilmaz, 2007). This means that above a certain LAI ($> 3 \ldots 5$) changes can be no longer detected. Another study by Hunt *et al.* (2011) concluded that changes in SWIR reflectance are not sufficiently responsive for water stress or water loss detection at LAI < 2.

Senescence of leaves When leaves are aging chlorophyll is decomposed. During this process carotenoids, which are also constituent parts of the photosynthesis apparatus, are not or only partially decomposed. As a result their characteristic yellow color appears as it is not longer overlaid with chlorophyll (Schopfer & Axel, 2010). In green vegetation carotenoids and chlorophyll exhibit strong and overlapping absorptions in the blue region of the electromagnetic spectrum which makes it difficult to separate their contribution to reflectance even at late stages of leaf senescence (Merzlyak & Gitelson, 1995; Gitelson & Merzlyak, 1994). Due to this overlapping absorption and reflection, indices which estimate the ratio of carotenoids to chlorophyll have been proved more successful than the estimation of the absolute carotenoid content (Merzlyak *et al.*, 1999; Peñuelas *et al.*, 1995). Merzlyak *et al.* (1999) describe the Plant Senescence Reflectance Index (PSRI) as a measure for the proportion between chlorophyll and carotenoids as a marker for senescence. Other indices which are based on the carotenoid absorption peak ($400 \ldots 500$ nm) are the 'structure insensitive pigment index' (SIPI), developed by Peñuelas *et al.* (1995) and the 'photochemical reflectance index' introduced by Gamon *et al.* (1992).

Sims & Gamon (2002) compared different carotenoid/chlorophyll ratio indices and reported that unlike to previous reports neither SIPI nor PSRI were significantly correlated with carotenoid/chlorophyll ratio.

Dry leave components The leaf reflectance spectrum is not only driven by water and chlorophyll content. Moreover lignin and cellulose, which are major components of leaves (Wessman *et al.*, 1988), play a role (Gao & Goetz, 1994). As mentioned, differences in foliar pigment levels would be indicative of the near-term growing environment, while remote sensing of canopy vigour based on estimates of struc-

tural chemical constituents allows forest health monitoring and damage detection of long-term environmental conditions (Campbell *et al.*, 2004). Lignin and cellulose absorption are overlaid by water absorption. Due to characteristic shapes of their absorption spectra they can be detected in the mid-infrared portion of the electromagnetic spectrum (Damm, 2008). Lignin and cellulose reflections can be used to distinguish non-photosynthetic vegetation from bare soil (Roberts *et al.*, 1993).

3.3.3. Remote sensing of forest health

Generally, remote sensing of forest condition underlies the same principles as remote sensing of vegetation condition. Components for stress detection are water content measures, lignin and cellulose reflection and of course the chlorophyll content together with carotenoid-chlorophyll ratios as indicator for photosynthetic activities. In case of a closed forest stand there are two complex systems which interact. Firstly, there is plant-physiology which has only few symptoms for many stressors and secondly there is physical behaviour of incoming electromagnetic radiation, which is in case of forests also very complex in itself.

Leaf pigments and internal structures The most sensitive indicators of short term plant stress, and with that forest stress, seem to be pigments (Campbell *et al.*, 2004; Lausch *et al.*, 2013). Many different broad and narrow band wavelengths were determined and directly linked to forest health status. Lausch *et al.* (2013) stated that especially chlorophyll absorbing bands are useful for forest health determination, whereas within the short-wave infrared no increased importance was measured. This matches with the statement of Campbell *et al.* (2004): A change in chlorophyll absorbency allows to detect near-term growing conditions. Differences in these items within a single species are indicative for differences in the health status (Campbell *et al.*, 2004).

Rough surface at canopy scale In addition to foliar pigments, water-content and other biochemical constituents, reflection properties of forests at canopy level are influenced by canopy density, structure and transmittance of the incoming radiation (Campbell *et al.*, 2004). If incoming electromagnetic waves are directly reflected by the leaves' surface, its pigments, water contents or structure do not play any role. If waves are transmitted, the LAI becomes important. Due to the multitude leaf layers which occur in a forest, parts of the electromagnetic radiation can be reflected and transmitted many times. Additionally some indices tend to saturate in higher LAI values. This may lead to undetectable changes which could be essential in early detection of changes in health status.

A good example for interaction between plant-physiology and leaf area index is described in Campbell *et al.* (2004): Due to the degree of canopy closure, two stands can have similar pigment concentrations per unit of leaf mass while they have different foliar pigment concentrations per unit of canopy area and vice versa.

Temperature Temperature of canopies might play a role as well since water stress leads to closure of stomata, less transpiration and finally higher temperatures. Sepulcre-Cantó *et al.* (2006) gives a good overview about methods and indices which can be used for water stress detection with thermal bands.

Compared to multispectral data it is absolutely possible to detect different stress stages at canopy scale with hyperspectral data. Campbell *et al.* (2004) stated that hyperspectral data can provide improved forest damage separation capacity when compared to multispectral broadband data. Basically, forests are complex structures on the plant-physiological level and on the physical reflection behavior side, with many of overlaying and influencing processes, which will always make it challenging to remotely detect changes.

4. Data acquisition and preparation

Data acquisition and preparation depicts where and how needle samples were taken. Furthermore the measurement procedure of needle reflectance spectra in the spectral laboratory is described.

4.1. Study area

Needle samples were taken in Bavaria, the most densely wooded federal state in Germany. More than a third (36.3%) of its land is covered with forest, an area of 25,610 km^2. This forest consists mainly of Norway Spruce (*Picea abies*) with 44.6%, which is much more than the average in Germany (28.2%). Other tree species in Bavaria are Scots pine (*Pinus sylvestris*) with 18,8%, Larch (*Larix decidua*) and Silver fir (*Abies alba*) with 2% each and Douglas fir (*Pseudotsuga menziesii*) with just 0.6%. But also deciduous tree species like Beech (*Fagus sylvatica*) with 12.2% and oak (Quercus petraea) with 6.1% can be found. Different other deciduous tree species make up another 12.7%.

The test site is located about 100 km east from Munich. It is managed by the forest holding 'Wassserburg am Inn', which is one of 41 forest districts of the Bavarian state forest.

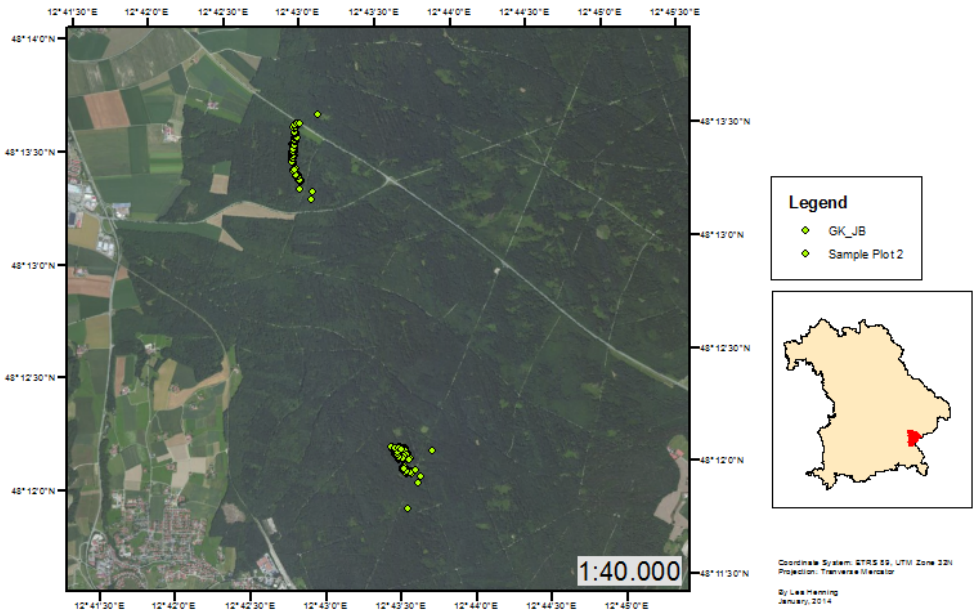

Figure 4.1.: Location of sample plots

Stand characteristics The chosen stands are dominated by Norway spruce with admixture of Scots pine between 10 and 30%. One is 60 and the other one 100 years old. As it is a planted forest stand it can be assumed that all trees within one section are of the same age. The forest holding 'Wassserburg am Inn' ranges from the sub-continental Munich gravel plain to the more continentally characterized lower Bavarian tertiary hill country. The mean annual temperature is 7.6°C, with a mean temperature of 14.9°C during the vegetation period. The average annual precipitation is between 850 and 950 mm, of which around 500 mm fall during the vegetation period. Site conditions are solid with dominating dry and mesic-moist soil conditions (Bayerische Staatsforsten, 2013).

4.2. Data acquisition

Measured were reflectance spectra of sprouts from the four last years of 8 ring-barked and 8 control trees per plot. Spectra were taken in the spectral laboratory of the DLR. Afterwards needle spectra had to be processed.

Needle sampling Needle sampling took place four times in both sample plots. The first sample was collected on the 18^{th} of July, the second on the 20^{th} of August, the third on the 10^{th} of September and the last one on the 12^{th} of November 2013. Trees were climbed up by tree climbers who cut down one or two branches. Samples from these branches were cut off by age class and sealed in labeled plastic bags. Over night the samples were cooled down to minimize biological processes within the needles.

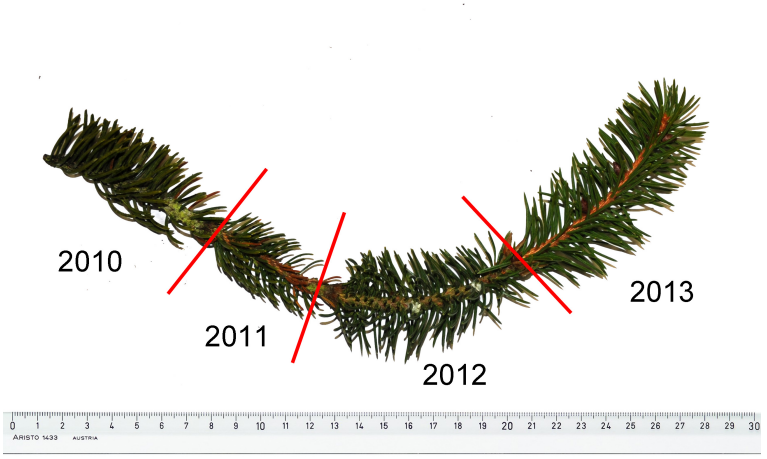

Figure 4.2.: Norway spruce twig with the last four age classes

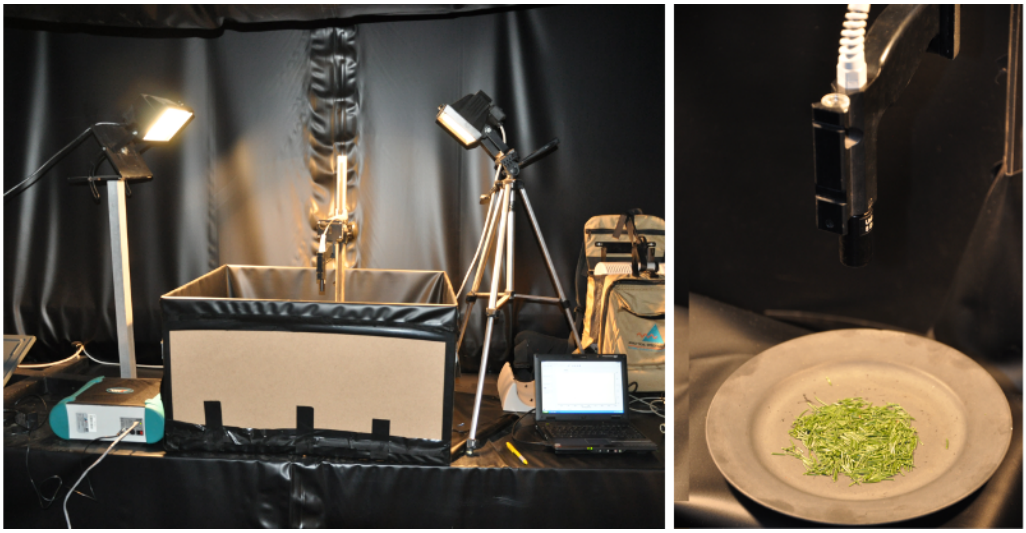

Figure 4.3.: Laboratory set-up for spectral measurements (photos: Tim Ng)

The needle age classes were defined by the sprouts, which can be easily differentiated at Norway spruce trees (figure 4.2). The youngest sprout, which grew during spring 2013 is defined as 'age class 1', the sprout which grew during spring 2012 was defined as 'age class 2', the sprout which grew during spring 2011 was defined as 'age class 3', the sprout which grew during spring 2010 was defined as 'age class 4'.

Laboratory spectral measurements Needle sample reflectance spectra were measured under controlled conditions to generate a dataset without influences by atmospheric conditions or illumination. Measurements were conducted with an ASD FieldSpec-Pro spectroradiometer which was equipped with an 8°-fore optic. The measurements range over the 350 to 2,500 nm wavelength region. Internally the laboratory is covered with matt black pond foil which has a continuously dark reflection and no significant absorption features (Bayer, 2013). For spectral analysis, the needles were cut off the twigs and placed on a dish covered with a matt black 3M varnish to minimize reflection. The applied measurement set-up is shown in figure 4.3. As light source served two Quartz halogen lamps with a power of 300 W each. Spectra were measured using a photodiode with field of view of 8° and with a distance of 15 cm between needle samplings and the detector. To obtain measurements between 300 nm and 2,500 nm it is equipped with three photodiodes. One for the visible electromagnetic range from 300 nm to 1,000 nm, and two for the short wave infrared range one from 1,001 nm to 1,800 nm and from 1,801 nm to 2500 nm (ASD Inc., 2013).

To account for illumination effects of needles, each measurement was repeated 8 times in between which was turned by 90°. For each plate position two measurements

were taken. Thus, in total 1024 single spectrum measurements per sample were taken (16 trees, 4 age classes of sprouts and 16 measurements each).

Between measurements the spectrometer needed to be calibrated with a Spectralon, which has a high and constant reflectance in the visible and infrared portion of the electromagnetic spectrum. It is used for calibration because changes in the surrounding of the spectrometer could lead to continual errors in measurements.

Spectra processing Laboratory spectra were corrected for the specific reflectance of the applied Spectralon reference panel. Spectral jumps between the wavelength range of each of the three ASD sensors (see fig. 4.4) were adjusted additively by taking the first detector as reference. Figure 4.4 shows one spectrum before and after jump correction. Especially between the bands 1000 and 1001 a jump is noticeable in the left image.

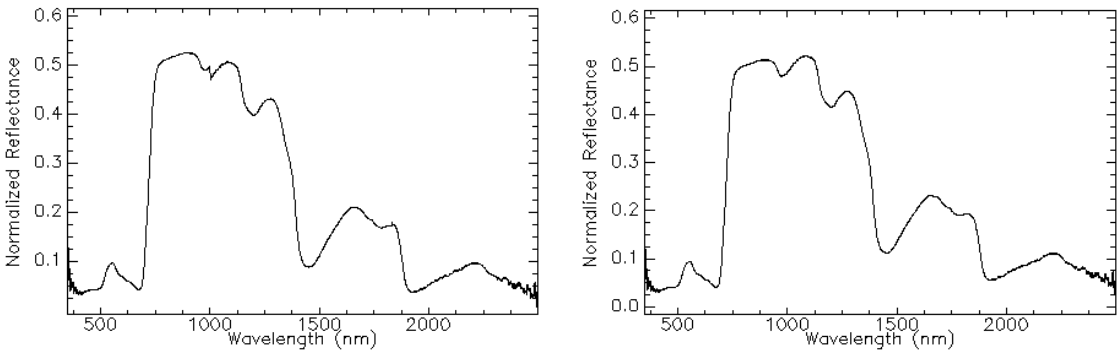

Figure 4.4.: Needle reflectance spectra before (left) and after (right) jump correction

Final data for statistical analysis After automatic processing of data, different spectra outputs were generated. An overview is given in table 4.1. There are the four samples from I to IV . Per sample, needles of 16 trees were collected (first column). Reflectance spectra were taken of the last four age classes of sprouts (1 to 4, first row) and measured 16 times per sampling. The final output for analysis were 16 corrected single spectra per age class and tree. Additionally a mean spectra was calculated out of the 16 single spectra.

The original electromagnetic range from 300 nm to 2,500 nm was limited due to increasing noise in boundary areas. It was set from 425 to 2450 nm. For analysis of data, the single spectra were used and a database was created which allowed differentiation between the sample plots (F1 and F2), between ring-barked and control trees (1 for ring-barked and 2 for control) and between the age classes (1 to 4).

Table 4.1.: Overview of final data for analysis

		age class 1		...	age class 4	
		single spectra	mean spectrum		single spectra	mean spectrum
Sample I	Tree 1	16	1	...	16	1
	⋮	⋮	⋮	...	⋮	⋮
	Tree 16	16	1	...	16	1
⋮		⋮	⋮		⋮	⋮
Sample IV	Tree 1	16	1	...	16	1
	⋮	⋮	⋮	...	⋮	⋮
	Tree 16	16	1	...	16	1

5. Methodology

Various approaches were applied to measure if and where differences between ring-barked and control tree reflectance spectra occur. Figure 5.1 gives an overview about the processes which were conducted. It describes the principal component analysis, as well as the derivative analysis and the Savitzky-Golay smoothing filter. Furthermore the applied indices are mentioned.

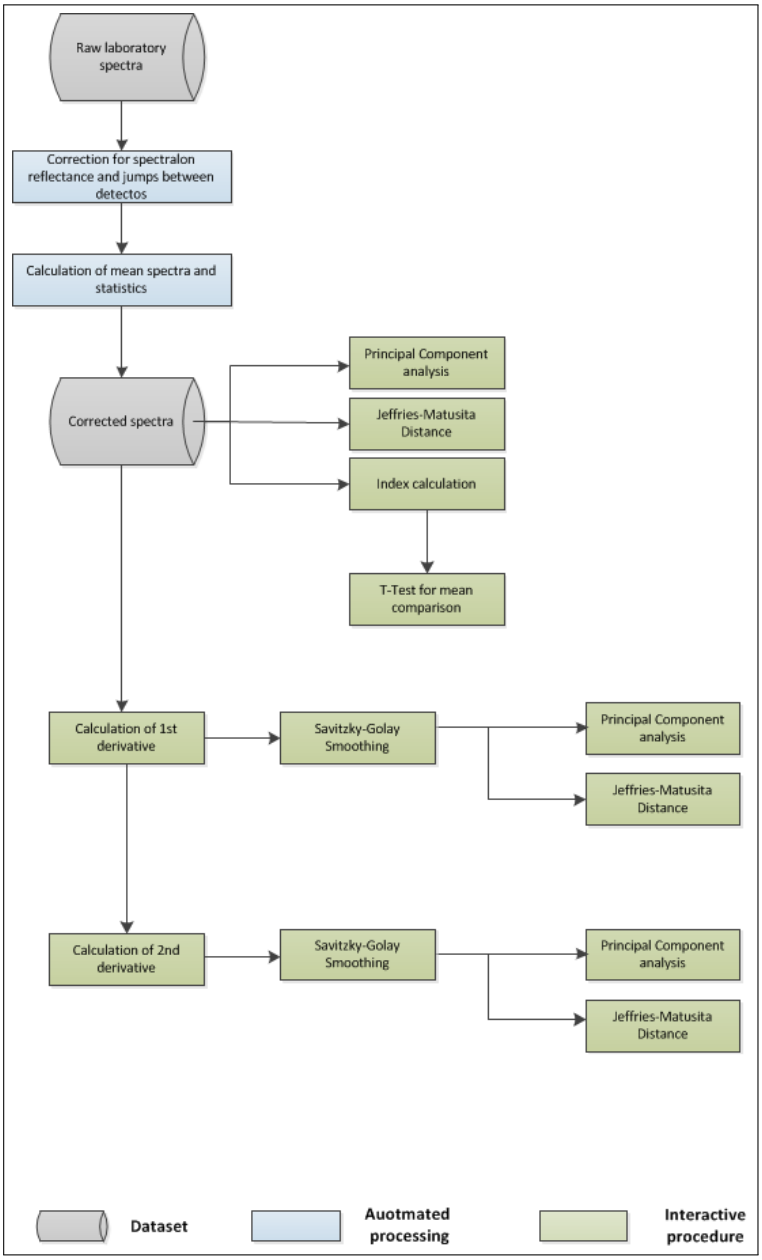

Figure 5.1.: Overview flow chart of conducted processes

5.1. Principal Component Analysis

The principal component analysis (PCA) is a multivariate method of statistical analysis and is widely used for multidimensional datasets in socioeconomics, biology, physics and remote sensing. It is used to find structures in data which are otherwise not easy to detect.

First of all, correlated data are converted to an uncorrelated dataset with less complexity. In this case a hyperspectral data cube with three dimensions (two space coordinates, one spectral coordinate) is transformed into a two-dimensional matrix. Then the covariance matrix can be calculated following eq. (5.1). This matrix serves as basis for calculation of eigenvectors. These again describe the variance wherein eigenvector 1 describes the largest variance in the data, eigenvector 2 the second largest and so on. The calculated eigenvectors can now be combined into a new matrix with which the new brightness values for the pixels in the principal axes can be calculated (Richards & Jia, 2006). For detailed information concerning principal component transformation see Richards & Jia (2006).

$$\Sigma_x = \frac{1}{K-1}\sum_{k=1}^{K}(x_k - m)(x_k - m)^t \tag{5.1}$$

The PCA was calculated for all samples together and per each sample. It plotted to get a first visual impression about the data. Obvious differences between the 'ring-barked' and 'control' group, should be visually detectable in the PCA of reflectance spectra

5.2. Jeffries-Matusita Distance

The Jeffries-Matusita (JM) distance is an often used indicator for separability between classes. It is asymptotic to the value 2 for increasing class separability and the measure of the average distance between the two class density functions. A JM distance of two between spectral classes would imply classification of those classes with 100% accuracy. Generally good separation between two classes can is possible when the JM distance is above 1.90, JM distance below 1.0 implies very poor separability between two classes (Richards & Jia, 2006). For this work the JM distance is applied to assess separability between ring-barked and control trees per sample. It was applied for each sample per year to account for the possibility, that changes which lead to separability between these classes occur only in one year. Bands for

JM distance calculation are directly linked to the health status of vegetation and were selected following the results described in the literature review (section 3.3). Six bands were chosen located in the green and red region, the red edge and infrared region of the electromagnetic waves as well as in the higher frequencies with lignin and cellulose reflections.

The JM distance calculation was based on eq. (5.2).

$$J_{ij} = \sqrt{2(1 - e^{-B})} \tag{5.2}$$

where

$$B = \frac{1}{8}(\mu_i - \mu_j)^T \left(\frac{\Sigma_i + \Sigma_j}{2}\right)^{-1} (\mu_i - \mu_j) + \frac{1}{2} ln \left(\frac{(1/2)|\Sigma_i + \Sigma_j|}{\sqrt{|\Sigma_i| x |\Sigma_j|}}\right) \tag{5.3}$$

The subscript i and j designate the signatures (classes) which are compared, Σ_i is the covariance matrix of signature i, μ_i is the mean vector of signature i, ln is the natural logarithm function, T means matrix transposition and $|\Sigma_i|$ is the determinant of Σ_i. With increasing class separation the JM distance has a saturating behavior (Richards & Jia, 2006).

As the JM distance is obtained from the Bhattacharyya (BH) distance, this is also reported in the output tables. For the BH distance a larger value indicates greater average distance although it not necessarily indicates how successful two classes are discriminated (Richards & Jia, 2006).

5.3. Derivative Analysis

In spectroscopy derivative analysis is used to sharpen spectral features or separating components which are clearer in the derivative spectrum than in the reflectance spectrum. Furthermore derivatives provide the advantage that second or higher order derivatives are relatively insensitive to illumination variations (Tsai & Philpot, 1998). Holden & LeDrew (1998) described that first order derivatives provide information about the rate of change in reflectance (changes in the slope) with respect to the wavelength.

First and second derivative of reflectance data were calculated with respect to the wavelength data analysis. Estimation for the first derivative is shown in eq. (5.4). Eq. (5.5) gives the 2^{nd} derivative.

$$\frac{dR}{d\lambda} = \frac{R(\lambda_j) - R(\lambda_i)}{\Delta\lambda} = R' \tag{5.4}$$

and

$$\frac{d^2R}{d\lambda^2} = \frac{d}{d\lambda}\left(\frac{dR}{d\lambda}\right) = \frac{R'(\lambda_j) - R'(\lambda_i)}{\Delta\lambda} = R'' \tag{5.5}$$

5.3.1. Savitzky-Golay filter

To improve derivative data which are sensitive to noise, smoothing was applied. In this case both derivatives were smoothed with a third order polynomial smoothing filter of 5 nm width (Savitzky & Golay, 1964). It offers sequential internal smoothing passes to improve overall noise reduction (Jonckheere *et al.*, 2005). The general equation of the least squares convolution can be given as follows:

$$I_i^* = \sum_{j=-m}^{j=m} C_j I_{i+j} \tag{5.6}$$

whereby I_i^* is the resultant value, C_j is the convolution coefficient for the filter value and I_i (i= 1,2,...,n) are the ongoing brightness values. The number of convolution integers is equal to the window size (2m+1) . For a smoothing filter with a window size of 5 data points, the convolution coefficients C_j are $[-3/35; 12/35; 17/35; 12/35; -3/35]$ (Jonckheere *et al.*, 2005).

5.4. Indices

Several different indices concerning the chlorophyll concentration, water content, leaf pigments and carbon in lignin form were evaluated. As described in section 3.3, indices can be used for many different purposes like detection of vegetation, land cover changes or soil type detection. In this case indices were used for differentiation within one class (Norway spruce).

Normalized Difference Vegetation Index The Normalized Difference Vegetation Index (NDVI) might be the most widely used vegetation index for assessing dynamics and the state of vegetation. It is based on a red band around 600 nm and a reference band from the near-infrared plateau (700 ... 1200 nm) (Herrmann *et al.*, 2010). With that it mainly describes photosynthetic activity (Clark *et al.*, 1993)

and can be applied for a lot of different multispectral sensor systems. The value of this index ranges from -1 to 1. The common range for green vegetation is 0.2 to 0.9.

$$NDVI = \frac{p_{800} - p_{670}}{p_{800} + p_{670}} \tag{5.7}$$

Red Edge Normalized Difference Vegetation Index For detection of changes in the chlorophyll content the Red Edge Normalized Difference Vegetation Index (RENDVI) was used. It was described by Gitelson & Merzlyak (1994) and uses bands along the red edge (705 nm and 750nm). Sims & Gamon (2002) described it to be sensitive to small scale changes in canopy chlorophyll content. Like the NDVI this index ranges from -1 to 1 and the common range for green vegetation is between 0.2 and 0.9 (Sims & Gamon, 2002).

$$RENDVI = \frac{p_{750} - p_{705}}{p_{750} + p_{705}} \tag{5.8}$$

Normalized Difference Water Index The Normalized Difference Water Index (NDWI) was described by Gao (1996). Both bands are located in the high reflectance plateau of vegetation canopies (857 nm and 1241 nm). It is described to be sensitive to changes in liquid water content of vegetation canopies and to be less sensitive to atmospheric effects than the NDWI (Gao, 1996). The NDWI ranges from -1 to 1 with a common range for green vegetation from -0.1 to 0.4 (Gao, 1996).

$$NDWI = \frac{p_{860} - p_{1240}}{p_{860} + p_{1240}} \tag{5.9}$$

Plant Senescence Reflectance Index Beside chlorophyll and water detection it is also possible to detect stress-related pigments like anthocyanins or carotenoids. They are present in higher concentrations in stressed vegetation (Gitelson *et al.*, 2001, 2002). Senescence-induced degradation of chlorophyll is accompanied by an increase of reflectance between 550 and 740 nm, whereas it remains low in the range between 400 and 500 nm, due to retention of carotenoids Merzlyak *et al.* (1999). The Plant Senescence Reflectance Index (PSRI) was found to be sensitive to the chlorophyll/carotenoids ratio. With that it could be used as a quantitative measure of leaf senescence. This index ranges from -1 to 1 and the common range for green vegetation is from -0.1 to 0.2 (Merzlyak *et al.*, 1999).

$$PSRI = \frac{p_{678} - p_{500}}{p_{750}} \tag{5.10}$$

Normalized Difference Lignin Index Carbon are included in vegetationin in different chemical compounds: starch, sugar, lignin or cellulose. While lignin is part of structural strong parts of plants, cellulose is included in cell walls of vegetation tissues. The less reflection is dominated by chlorophyll or water content, the more reflections of other compartments can be observed (Gao & Goetz, 1994). These reflection characteristics make it possible to distinguish between fallow land and dead or dry vegetation. In this case the Normalized Difference Lignin Index was used. The included band at 1754 nm is primarily determined by lignin concentration of the canopy. The value of this index ranges from 0 to 1 while the common range for green vegetation is between 0.005 and 0.05 (Serrano *et al.*, 2002).

$$NDLI = \frac{log(1/p_{1754}) - log(1/p_{1680})}{log(1/p_{1754}) + log(1/p_{1680})} \tag{5.11}$$

5.5. Unpaired samples t-test

The unpaired samples t-test gives the possibility to check whether two groups are different concerning an attribute. It provides decision support if a difference found between mean values is random or not. Mathematically written it calculates whether there is a systematic difference between two mean values or not (for detailed information about the unpaired samples t-test see Bortz (1989)). In this case it was used with the null-hypothesis, that both samples come from populations in which parameter μ_1 and μ_2 are identical.

$H_0 \quad : \quad \mu_1 - \mu_2 = 0$
$H_1 \quad : \quad \mu_1 - \mu_2 \neq 0$

The t-test has the preconditions that there is normal distribution of the data and homogeneity of variance. Normal distribution can be assumed as the t-test is robust against not perfectly normally distributed data (Guiard & Rasch, 2004) and due to the central limit theorem the data are nearly normally distributed (Bortz, 1989). Furthermore the t-test is robust against variance heterogeneity if the sample size is equal (Guiard & Rasch, 2004) which is the case for the evaluated data.

The two sample t-test for unpaired data is defined as:

$$t = \frac{\bar{x}_1 - \bar{x}_2}{\hat{\sigma}_(\bar{x}_1 - \bar{x}_2)} \quad , \tag{5.12}$$

with

$$\hat{\sigma}_{(}\bar{x}_1 - \bar{x}_2) = \sqrt{\frac{\hat{\sigma}_1^2}{n_1} + \frac{\hat{\sigma}_2^2}{n_2}} \tag{5.13}$$

$\bar{x}_1$	:	Mean value of sample I
$\bar{x}_2$	:	Mean value of sample II
$\hat{\sigma}_{(}\bar{x}_1 - \bar{x}_2)$	:	Estimated standard deviation of mean difference
n_1	:	Number of observations in sample I
$\hat{\sigma}_1^2$	:	Estimated variance of population 1
n_2	:	Number of observations in sample II
$\hat{\sigma}_2^2$	:	Estimated variance of population 2

5.6. Paired samples t-test

As the unpaired samples t-test, the paired samples t-test is used to check whether two groups are different concerning an attribute. In contrast to the unpaired samples t-test this test can be used if measurements were repeated and dependent measurement pairs occur: For example the health status before and after a treatment. This test considers that variance of sample I might influence the variance of sample II or vice versa (for detailed information about the unpaired samples t-test see Bortz (1989)).

The paired samples t-test is defined as:

$$t = \frac{\bar{x}_d}{\hat{\sigma}_{\bar{x}_d}} \quad , \tag{5.14}$$

with

$$\hat{\sigma}_{\bar{x}_d} = \frac{\hat{\sigma}_d}{\sqrt{n}} \quad . \tag{5.15}$$

$\bar{x}_d$	:	Arithmetic mean of differences between each pair of measurement
$\hat{\sigma}_{\bar{x}_d}$	:	Standard deviation of the distribution of $\bar{x}_d$
$\hat{\sigma}_d$	:	Estimated variance of differences in the population

6. Results

This chapter summarizes results of the principal component analysis, the Jeffries-Matusita distance as well as the index and t-test results.

For a first step, only sample I (18th of July) and sample IV (12th of November 2013), which was sampled last, have to be taken into account for the analysis. This is sufficient to investigate, whether changes in reflectance spectra are detectable at all. The other samples may be of interest in a second step, to analyze if the determined change might be detectable at an earlier point in time.

For the sake of completeness all result tables which are not discussed in detail are attached in the appendices.

6.1. Reflectance spectra

Mean needle reflectance spectra of sample I and IV are shown in figure 6.1, where the reflectance spectra of ring-barked trees are colored red and spectra of control trees are colored black. Needle reflectance spectra of sample I (18th of July, see section 4.2) are shown on the left side while the reflectance spectra of sample IV (12th of November 2013, see section 4.2) are displayed on the right side. In sample I all the reflectance spectra lie close together in the visible range and above 1,400 nm. Only in the range between 700 nm and 1,400 nm the reflectance spectra vary largely. Visually it is not possible to distinguish between ring-barked and control trees. In sample IV reflectance spectra lie still close together in the visible range but a small increase in variance above 1,400 nm can be detected visually. Furthermore the right chart (sample IV) contains outliers. In the red region (600 to 700 nm) two trees (ring-barked and control) show increased reflection as well as one tree (control group) shows increased reflection behavior in the short wave infrared region above 1,400 nm.

Between sample I (left chart) and sample IV (right chart) small differences in reflection behavior of the measured needle reflectance spectra are visible but these changes do not seem sufficient for a visual differentiation possibility of those two groups.

Age class 3 changed their color during the five months of the experiment in both groups, control and ring-barked trees, which was clearly noticeable in the spectra in sample IV . An example is given in figure 6.2. It shows a typical reflectance spectrum of healthy, green vegetation (solid line) with low reflectance in the blue and red range of the electromagnetic waves and high reflectance values in the near-

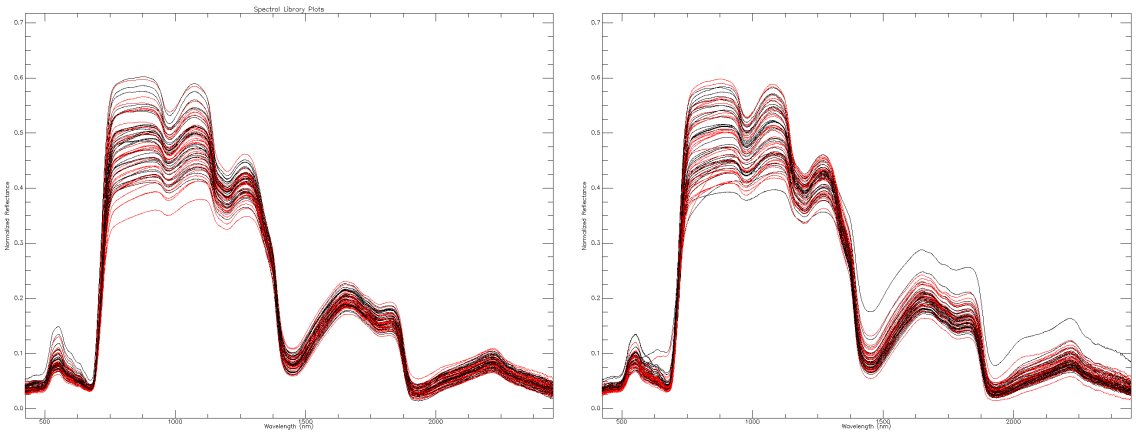

Figure 6.1.: Mean needle reflectance spectra of sample I (left, 18th of July) and sample IV (right, 12th of November 2013); red = ring-barked trees, black = control trees

infrared which was measured from age class 2 needles of a specimen in sample IV . The dotted line shows a typical reflectance spectrum of discolored vegetation which was measured from age class 3 needles from the same sample. Chlorophyll absorption decreased especially in the red portion of the electromagnetic spectrum, as well as the reflectance in the near-infrared decreased while reflection in the range between 1300 nm and 2400 nm increased.

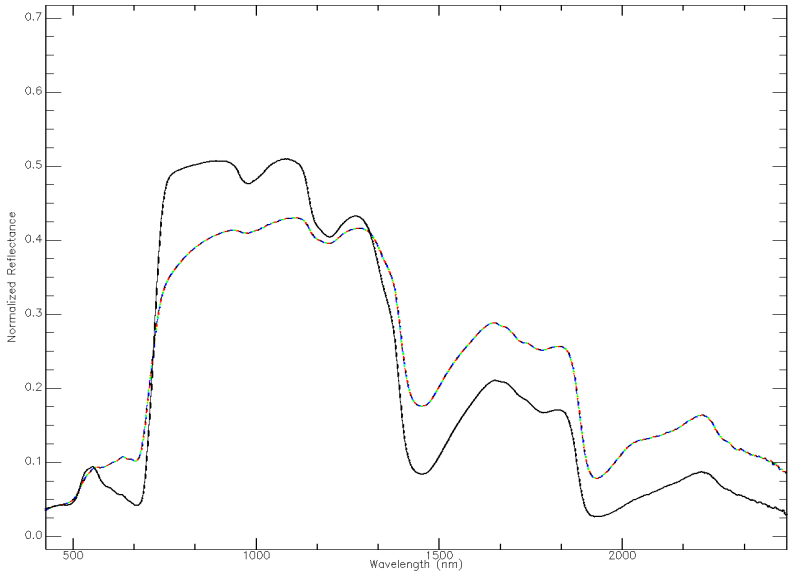

Figure 6.2.: Mean reflectance curves of sample IV for healthy age class 2 needles (solid line) and aged age class 3 needles (dashed line)

6.2. Survey of data with the principal component analysis

Principal component analysis for reflectance data was done for all reflectance spectra, separately by sample (I , II , III , IV) and differentiated by shoots of the last four years (1, 2, 3, 4). Results for sample I and IV are discussed here, results for sample II and III can be found in the appendix A.

6.2.1. Principal component analysis with reflectance data

PCA for all spectra Figure 6.3 displays the result of the first and second principal component with all spectra from sample I , II , III and IV , including all needle age classes. All four charts show the same data cloud (first and second principal components) with different illustrations, For detecting differences between the sampling areas, the data were initially split by sample plot (for plot description see section 4.1, top left). The result shows that there is no obvious difference between both areas and they can be handled as one dataset in the following. In the second plot (top right) data were split by sample to check whether spectra are noticeably changing within the vegetation period. Again the result of the first two PCAs does not show significant differences in the spectra. The third figure (bottom left) shows data split by ring-barked and control trees. A clear differentiation or trend which makes it possible to distinguish between ring-barked and control trees is not visible. Finally the fourth figure (bottom right) shows the data split by age class (see table 4.1). This is the only plot in which it is noticeable that shoots of age class 1 and 2 can be distinguished from shoot of age class 3 and 4. Some outliers are visible, which belong to a control tree of area one of sample IV .

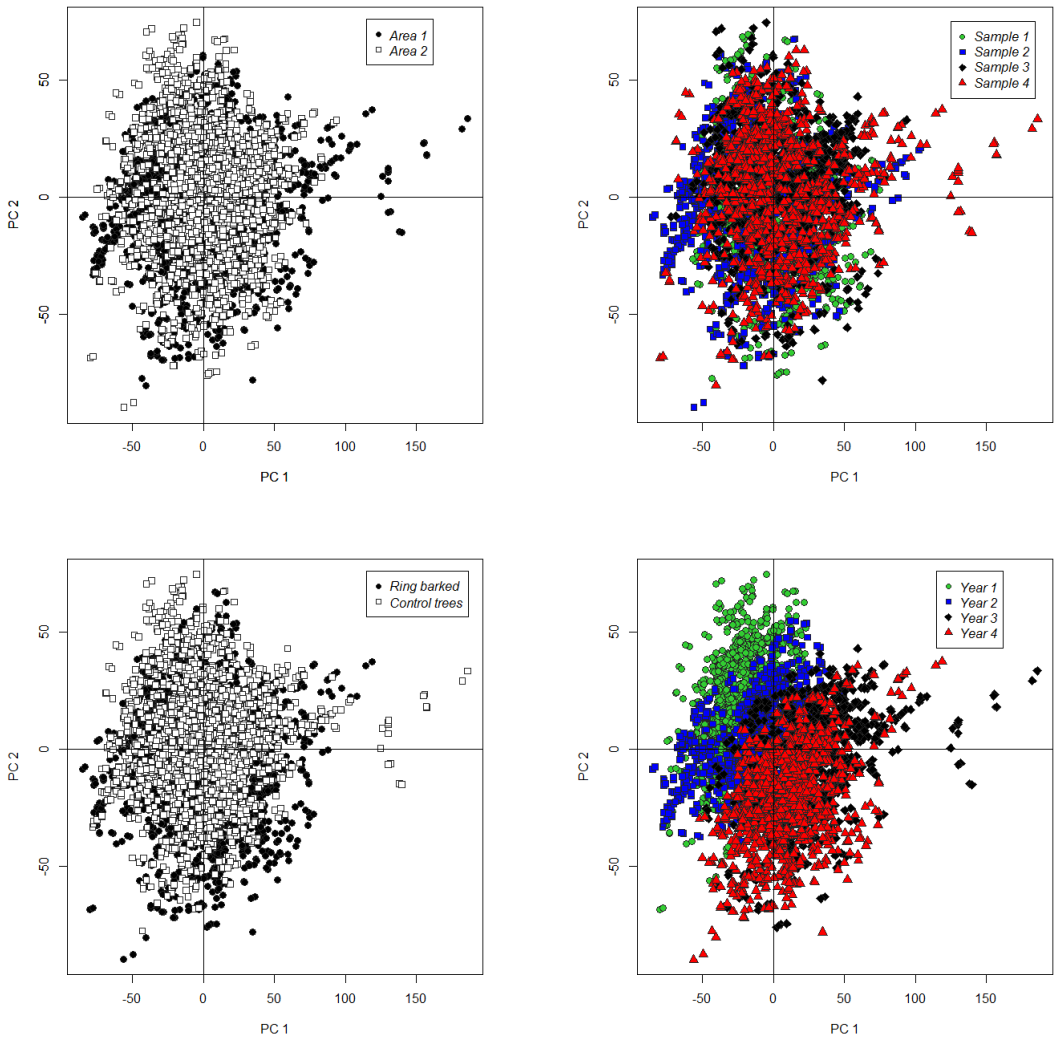

Figure 6.3.: Principal component analysis, using first and second principal components, for all reflectance spectra (sample I to IV), split by experimental side (top left), by sample (top right), by ring-barked and control trees (bottom left) and by age class (bottom right)

PCA for sample I and IV After analyzing the reflectance data as a whole dataset, the samples were evaluated per sample to check whether within one sample differences between the area, age classes and ring-barked and control trees occur. Figure reffig:samp1and4 displays the first two principal components for sample I (left) and IV (right). First plot of sample I (left side) displays data split by sample plot (area one and two). No difference between both areas can be noticed visually. The same applies to the first plot of sample IV (left). Both samples show no difference between plots. Charts in the second row display data split by ring-barked and control trees. It is not possible to distinguish between ring-barked and control trees with the first two principal components, neither in sample I nor in sample

IV . The last two plots in the third row display data split by age classes. In both samples it is possible to distinguish between age class groups 1/2 and 3/4.

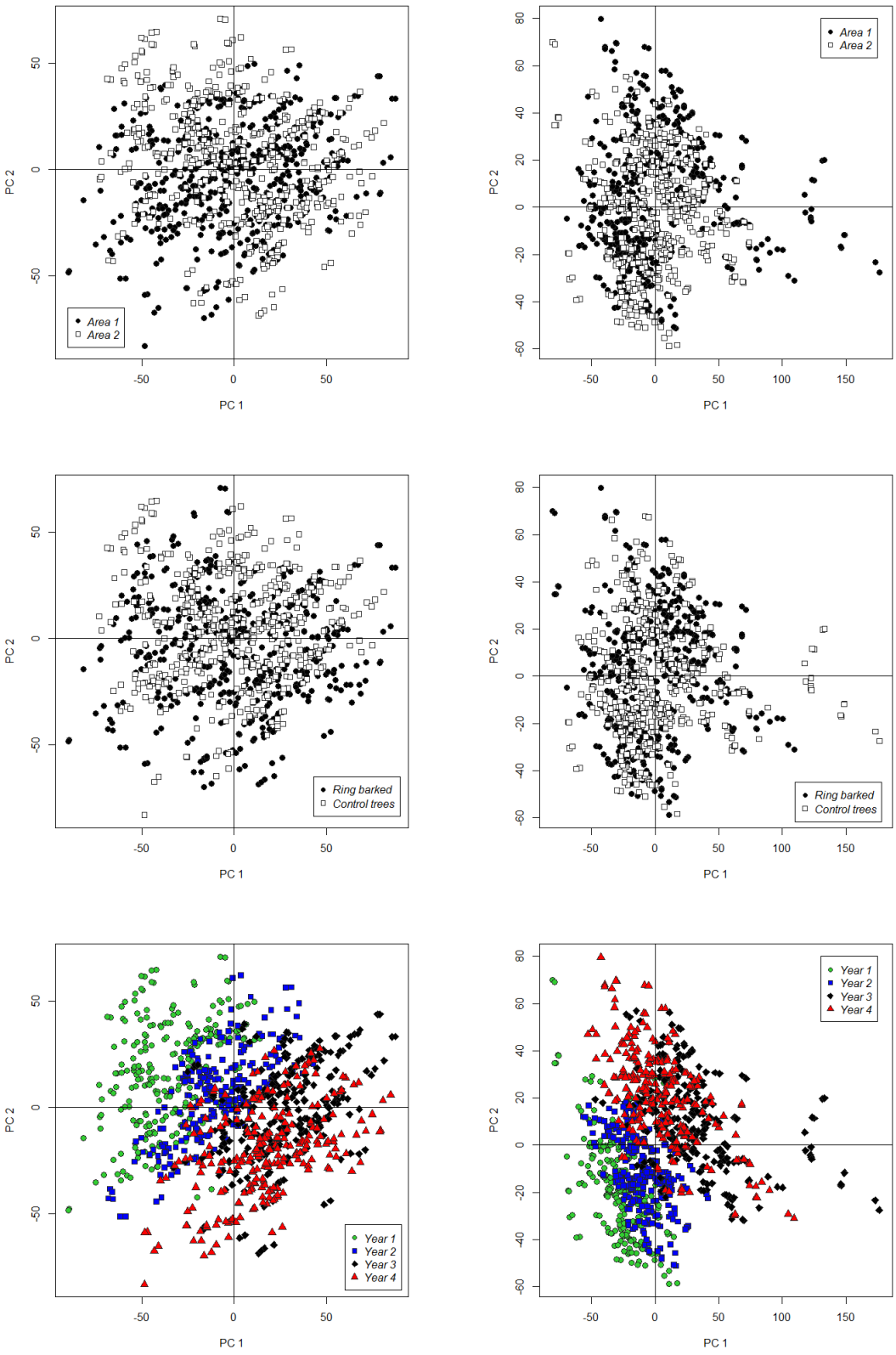

Figure 6.4.: Principal component analysis for sample I (left side) and sample IV (right side), split by area (top), ring-barked and control trees (middle) and age class (bottom)

PCA for age class 1 and 2 Finally age class 1 and 2 were analyzed separately from age class 3 and 4 for small scale changes within the reflectance spectra, which allow a differentiation between ring-barked and control trees. Figure 6.5 shows the PCA for spectra of only age class 1 and 2. Data were split by ring-barked and control trees (left) and by sample (right). The first chart (left) shows, that no differentiation between ring-barked and control trees is possible with the first two principal components of reflectance spectra of age class 1 and 2. The second chart (right) illustrates furthermore, that a differentiation between the samples is also not possible with the first two principal components of age class 1 and 2.

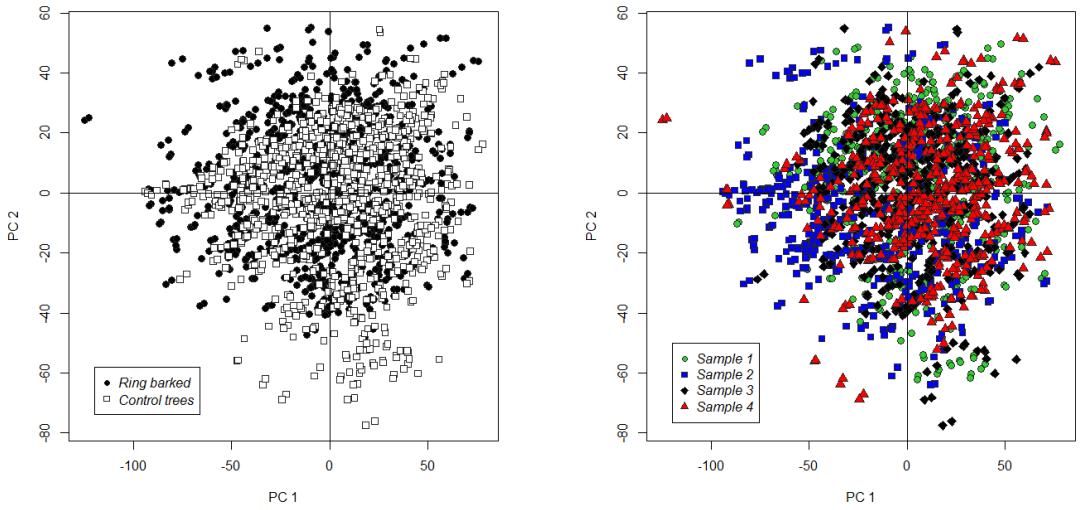

Figure 6.5.: PCA of age class 1 and 2, split by ring-barked and control trees (left) and by sample (right) for all four samples

6.2.2. Principal component analysis with derivative data

Figure 6.6 shows the same arrangement of charts like figure 6.3 but in this case with the PCA of derivative one.

Data are again plotted by area (top left), by sample (top right), by ring-barked and control group (bottom left) and age class (bottom right). Like the PCA plots with reflectance spectra these plots show no trends at the first sight. No difference between the areas, no clear changes between sample I and IV can be mentioned. Also no trend is detectable between ring-barked and control trees and finally sprouts of age class 1 and 2 can not be distinguished as well as 1 and 2 can be distinguished from 3 and 4 (see fig. 6.3)

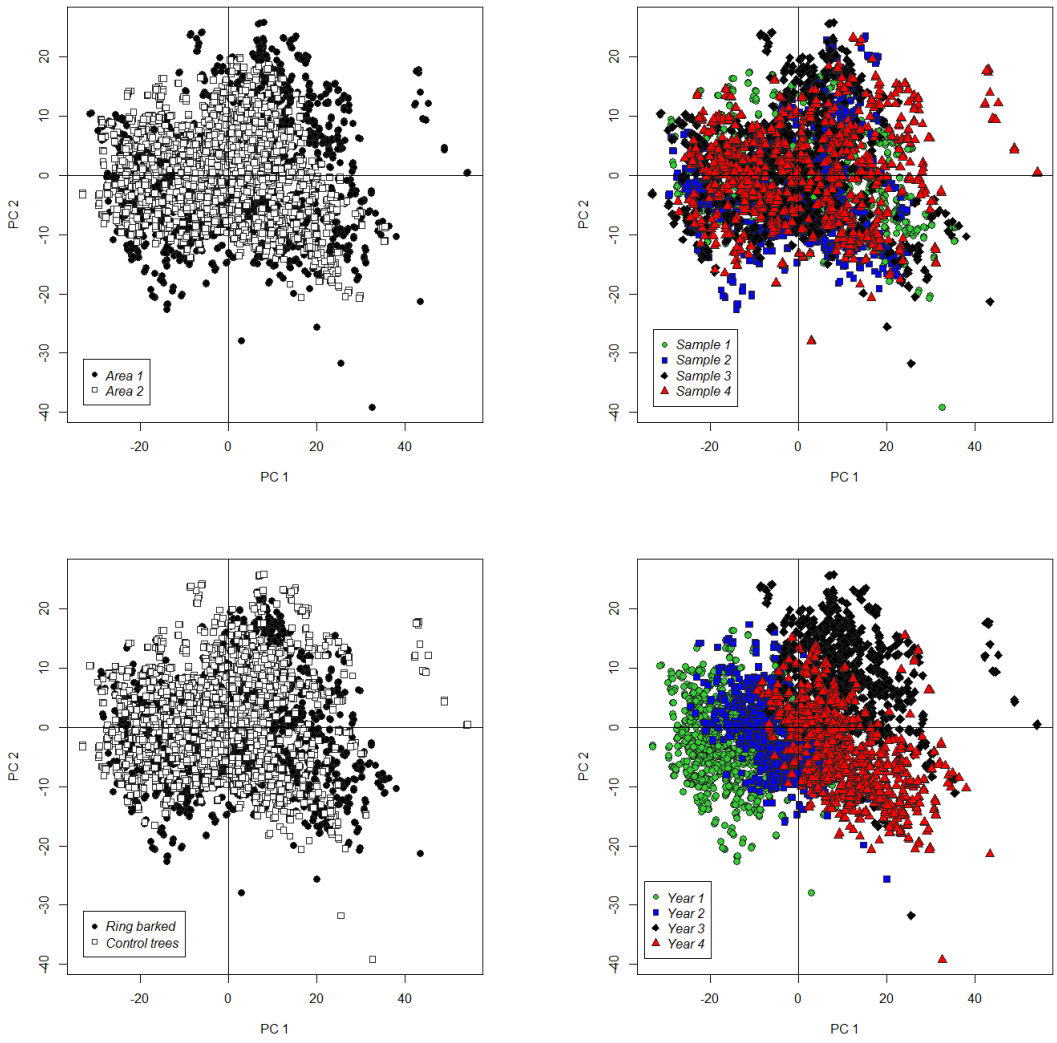

Figure 6.6.: Principal component analysis for 1^{st} derivative of all reflectance spectra split by experimental side (top left), by sample (top right), by ring-barked and control trees (bottom left) and by age class (bottom right)

The principal component analysis was also applied for the second derivative. Certainly with the same results. Charts with the first two principal components for all samples together are displayed in appendix A.2.

6.3. Distinction of ring-barked and control trees with Jeffries-Matusita Distance

The Jeffries-Matusita distance was calculated for sample I , II , III and IV between ring-barked and control trees. Tables show the JM distance split by age class (1, 2, 3, 4) and ring-barked (r) and control (c) trees. It was calculated with a subset of bands

which are linked to health status changes of vegetation (see section 3.3). Bands at 600 nm and 650 nm are located in the red portion of the electromagnetic radiation and with that strongly linked to chlorophyll activity, bands at 705 nm and 750 nm are located around the red edge which is linked to the health status of vegetation as well (see section 3.3), the band at 1241 nm is linked to water absorption (Gao, 1996) and the band at 1754 nm is linked to lignin absorption (Serrano *et al.*, 2002).

6.3.1. Jeffries-Matusita Distance for reflectance data

As written in chapter 5, a JM distance ≥ 1.90 stands for good separability while a JM distance of ≤ 1.00 stands for poor separability. Highlighted are the JM distances, which show the separability between ring-barked and control trees per age class. Table 6.1 and 6.2 show the JM distance for sample I and IV , ring-barked (r) and control trees (c) and per age class (1, 2, 3 and 4). JM distances for sample II and III are listed in appendix B.1.

Table 6.1.: Jeffries-Matusita Distance for reflectance spectra of sample I with the bands 600, 650, 705, 750, 1241 and 1754 nm.

	1r	1c	2r	2c	3r	3c	4r	4c
1r		**1.00**	1.90	1.95	2.00	2.00	2.00	2.00
1c	0.70		1.85	1.90	2.00	1.99	1.99	2.00
2r	3.04	2.62		**0.99**	1.91	1.79	1.95	1.89
2c	3.60	3.01	0..68		1.99	1.95	2.00	1.98
3r	14.56	7.02	3..14	5.76		**0.88**	0.78	0.77
3c	11.48	5.28	2..27	3.63	0.56		1.33	1.10
4r	10.81	5.75	3.74	6.04	0.49	1.10		**1.18**
4c	12.31	6.60	2.28	4.64	0.48	0.80	0.89	

Table 6.2.: Jeffries-Matusita Distance for sample IV , with the bands 600, 650, 705, 750, 1241 and 1754 nm.

	1r	1c	2r	2c	3r	3c	4r	4c
1r		**0.89**	1.88	1.93	1.99	1.96	1.93	1.95
1c	0.59		1.80	1.81	2.00	1.99	2.00	1.99
2r	2.79	2.30		**0.75**	1.99	1.94	1.95	1.84
2c	3.32	2.37	0.47		1.98	1.86	1.96	1.84
3r	4.95	8.51	5.88	4.41		**1.17**	1.33	1.37
3c	3.91	5.85	3.51	2.65	0.88		1.59	1.57
4r	3.41	6.51	3.66	3.92	1.10	1.59		**1.13**
4c	3.70	5.72	2.54	2.50	1.16	1.53	0.83	

JM distance for sample I Table 6.1 shows the JM distances for sample I . All four age classes have a JM distance, between ring-barked and control group, of around 1.0. Age class 1 has a JM distance of 1.00, age class 2 has 0.99, age class 3 has 0.88 and age class 4 has 1.18. Following the interpretation of the JM distance a very poor differentiation between ring-barked and control trees within the age classes is possible.

In addition the JM distance shows values ≥ 1.90 between the age classes. Values of 2.0 were calculated between age class 1 ring-barked and age class 3 (ring-barked and control) as well as age class 4 (ring-barked and control). Likewise high JM distances were calculated between age class 1 control and age class 3 (ring-barked and control) and age class 4 (ring-barked and control). These high JM distances reflect the visually interpreted results of the PCA. A differentiation between ring-barked and control trees is not possible. In contrast age classes can be differentiated, especially 1 and 2 against 3 and 4.

JM distance for sample IV The JM distances for sample IV (table 6.2), which was the last one, shows values around 1.0 for the separation between ring-barked and control trees. A JM distance of 0.89 for age class 1, 0.75 for age class 2, 1.17 for age class 3 and 1.13 for age class 4 between ring-barked and control trees implies again a poor separation between the classes ring-barked and control within all four age classes.

Furthermore high JM distance values were calculated between the age classes. 1.99 respectively 1.93 between age class 1 ring-barked and age class 3 (ring-barked and control) show good separability. High JM distance values of 1.99 respectively 1.95

between age class 2 ring-barked and age class 3 (ring-barked) or age class 4 (ring-barked) show again good separability between the age classes.

These findings of good separability between age classes and insufficient differentiation between ring-barked and control trees can be observed in all four samples. The JM distance tables for sample II and III can be found in the appendix B.1.

6.3.2. Jeffries-Matusita Distance for derivative data

JM distance was also calculated for derivative one and two of reflectance spectra. As example again sample I and IV are displayed.

6.3.2.1. JM distance for first derivative

Table 6.3.: Jeffries-Matusita Distance for derivative one of sample I , split by age class with the bands 600, 650, 705, 750, 1241 and 1754 nm. The upper right side shows the Jeffries-Matusita distance, the lower left side shows the Bhattacharyya Index

	1r	1c	2r	2c	3r	3c	4r	4c
1r		**0.32**	1.22	1.09	1.40	1.40	1.79	1.53
1c	0.18		1.55	1.35	1.69	1.64	1.91	1.75
2r	0.94	1.49		**0.29**	0.29	0.20	0.76	0.30
2c	0.79	1.13	0.16		0.55	0.24	1.29	0.63
3r	1.20	1.86	0.16	0.32		**0.26**	0.55	0.45
3c	1.20	1.72	0.10	0.13	0.14		0.87	0.28
4r	2.25	3.12	0.48	1.03	0.32	0.57		**0.63**
4c	1.46	2.08	0.16	0.38	0.25	0.15	0.38	

Table 6.4.: Jeffries-Matusita Distance for derivative one of sample IV , split by age class with the bands 600, 650, 705, 750, 1241 and 1754 nm. The upper right side shows the Jeffries-Matusita distance, the lower left side shows the Bhattacharyya Index

	1r	1c	2r	2c	3r	3c	4r	4c
1r		**0.24**	0.93	0.87	1.60	1.21	1.43	1.50
1c	0.13		0.64	0.59	1.32	1.08	1.21	1.26
2r	0.63	0.38		**0.16**	0.99	1.01	1.08	0.97
2c	0.57	0.35	0.09		1.07	1.01	1.10	1.07
3r	1.60	1.08	0.68	0.77		**0.41**	0.61	0.45
3c	0.93	0.78	0.70	0.70	0.23		0.49	0.68
4r	1.26	0.93	0.78	0.80	0.36	0.28		**0.43**
4c	1.39	0.99	0.67	0.77	0.25	0.42	0.24	

JM distance for sample I Table 6.3 shows the JM distance results for derivative one of reflectance spectra. Only between age class 1 (control) and age class 4 (ring-barked) a JM distance of above 1.90 was calculated. Within age classes JM distance values are very low. Values of 0.32 in age class 1, 0.29 in age class 2, 0.26 in age class 3 and 0.63 in age class 4 show poor differentiation possibilities within one age class between ring-barked and control trees. However, comparatively high JM distances were calculated between the age classes. 1.69 for age class 1 (control) and age class 3 (ring-barked), 1.79 for age class 1 (ring-barked) and age class 4 (ring-barked) or 1.29 for age class 2 (control) and age class 4 (control).

JM distance for sample IV JM distance values for first derivative of reflectance spectra of sample IV are displayed in table 6.4. JM distance values are similar to JM distance values of sample I . Values of 0.24 in age class 1, 0.16 in age class 2, 0.41 in age class 3 and 0.43 in age class 4, imply poor separation possibilities between ring-barked and control trees. Higher JM distance values were calculated between age classes, although no values > 1.90 are displayed.

JM distance tables for sample II and III are listed in appendix B.2.

6.3.2.2. JM distance for second derivative

Table 6.5.: Jeffries-Matusita Distance for derivative two of sample I , split by age class with the bands 600, 650, 705, 750, 1241 and 1754 nm. The upper right side shows the Jeffries-Matusita distance, the lower left side shows the Bhattacharyya Index

	1r	1c	2r	2c	3r	3c	4r	4c
1r		**0.16**	0.57	0.56	0.31	0.30	0.26	0.21
1c	0.09		0.48	0.48	0.32	0.34	0.34	0.27
2r	0.34	0.27		**0.20**	0.72	0.61	0.65	0.45
2c	0.33	0.28	0.11		0.68	0.57	0.57	0.42
3r	0.17	0.18	0.45	0.41		**0.15**	0.29	0.42
3c	0.16	0.19	0.36	0.34	0.08		0.23	0.32
4r	0.14	0.19	0.39	0.34	0.16	0.12		**0.18**
4c	0.11	0.14	0.25	0.23	0.24	0.17	0.09	

Table 6.6.: Jeffries-Matusita Distance for derivative two of sample IV , split by age class with the bands 600, 650, 705, 750, 1241 and 1754 nm. The upper right side shows the Jeffries-Matusita distance, the lower left side shows the Bhattacharyya Index

	1r	1c	2r	2c	3r	3c	4r	4c
1r		**0.26**	0.33	0.18	0.48	0.64	0.13	0.14
1c	0.14		0.35	0.24	0.67	0.78	0.29	0.16
2r	0.18	0.19		**0.21**	0.60	0.70	0.32	0.24
2c	0.09	0.13	0.11		0.55	0.67	0.24	0.18
3r	0.27	0.41	0.35	0.32		**0.10**	0.36	0.54
3c	0.38	0.50	0.43	0.41	0.05		0.43	0.63
4r	0.07	0.16	0.17	0.13	0.20	0.24		**0.15**
4c	0.07	0.08	0.13	0.10	0.31	0.38	0.08	

JM distance for sample I JM distance values for 2^{nd} derivative of reflectance spectra are displayed in table 6.5. JM difference values of 0.16 in age class 1, 0.20 in age class 2, 0.15 in age class 3 and 0.18 in age class 4 imply low separability between ring-barked and control trees with the 2^{nd} derivative. No JM distance > 1.00 was calculated, not even between the age classes. The highest JM difference of 0.72 was calculated between age class 2 (ring-barked) and age class 3 (ring-barked).

JM distance for sample IV Table 6.6 displays JM distance values, calculated with the 2^{nd} derivative of reflectance spectra. Separation between ring-barked and control trees is not determined as values of 0.26 in age class 1, 0.21 in age class 2, 0.10 in age class 3 and 0.15 imply poor separation. No JM distance value above 1.00 was calculated which suggests no differentiation between age classes.

JM distance tables for sample II and III can be found in appendix B.3.

6.4. Distinction between ring-barked and control trees with indices

Five indices were calculated. The paired and unpaired sample t-test was conducted to compare the mean index values between ring-barked and control group as well as between different points of time.

Table 6.7.: Mean index values for sample one to sample IV . 'R' = Ring-barked group; 'C' = Control group

	Sample 1	Sample 2	Sample 3	Sample 4
NDVI	R=0.85	R=0.85	R=0.85	R=0.84
	C=0.85	C=0.85	C=0.85	C=0.83
RENDVI	R=0.56	R=0.55	R=0.54	R=0.53
	C=0.56	C=0.55	C=0.54	C=0.53
NDWI	R=0.08	R=0.09	R=0.09	R=0.08
	C=0.09	C=0.09	C=0.10	C=0.09
NDLI	R=0.048	R=0.048	R=0.047	R=0.047
	C=0.048	C=0.048	C=0.048	C=0.047
PSRI	R=-0.01	R=-0.01	R=-0.01	R=0.004
	C=-0.01	C=-0.01	C=-0.01	C=0.001

Table 6.7 shows the mean index values of all five indices and all four samples split by ring-barked and control trees.

The **NDVI** values are with values between 0.85 and 0.84 in both groups in all four samples within the range of green vegetation (0.2 to 0.9). A slight decrease can be observed in sample IV but in both groups. Also the **RENDVI** mean values show in all four samples the same mean values for the ring-barked and control group, within the range for green vegetation which is from 0.2 to 0.9. Again a slight decrease in the index values can be observed in both groups in sample IV . The **NDWI** mean values are not as constant as the NDVI and RENDVI mean values and differ slightly during the measurement period. These changes can be observed in both groups and no differentiation between ring-barked and control trees can be observed. Furthermore these changes occur within the range of green vegetation (-0.1 to 0.4). Like the other three indices the **NDLI** values are within the range of green vegetation (0.005 to 0.05). Nearly no changes can be observed during the measurement period only the control group shows a slight change in sample IV . Finally the **PSRI** index is also within the range of green vegetation which is between -0.1 and 0.2. Nevertheless this index shows the biggest change from -0.0101 in sample I for the ring-barked group to 0.0040 in sample IV . This increase in the index mean value could also be observed for the control group but not as high as in the ring-barked group (from -0.0115 in sample I to 0.0013 in sample IV).

Table 6.8 shows the index mean values for age class 1 in all four samples split by ring-barked and control trees. Index values are generally slightly higher than in

table 6.7. Slightly higher index values can be observed in age class 2, 3 and 4, too. Small up and downturns can be observed within all spectra split by ring-barked and control groups (tab. 6.7) and in the index mean values of the single age classes (see appendix C.2 for mean values for indices per age class).

Table 6.8.: Mean index values for sample I to sample IV of age class 1 with 'R' = Ring-barked group; 'C' = Control group

	Sample 1	Sample 2	Sample 3	Sample 4
NDVI	R=0.86	R=0.87	R=0.86	R=0.87
	C=0.86	C=0.86	C=0.86	C=0.87
RENDVI	R=0.57	R=0.57	R=0.55	R=0.56
	C=0.54	C=0.57	C=0.55	C=0.57
NDWI	R=0.13	R=0.13	R=0.13	R=0.13
	C=0.13	C=0.14	C=0.14	C=0.13
NDLI	R=0.051	R=0.050	R=0.050	R=0.049
	C=0.051	C=0.050	C=0.051	C=0.050
PSRI	R=-0.02	R=-0.02	R=-0.02	R=-0.01
	C=-0.02	C=-0.02	C=-0.02	C=-0.02

Summarized all indices, independent of age class or group, are within their range for green and healthy vegetation. No considerable trend can be observed neither between sample I and IV nor between ring-barked and control trees.

6.4.1. Unpaired sample t-test

The independent samples t-test was conducted to compare index mean values of ring-barked and control trees, to differentiate between both groups.

Table 6.9.: T-test results for differences between mean index values of 'ring-barked' and 'control' group in sample IV . N.s. = not significant

	Sign.
NDVI	$t(1022) = 1.332, n.s.$
RENDVI	$t(1022) = -0.055, n.s.$
NDWI	$t(1022) = -1.903, n.s.$
NDLI	$t(1022) = -0.380, n.s.$
PSRI	$t(1022) = 1.242, n.s.$

Table 6.9 shows the t-test results for index mean value comparison between ring-barked and control trees for each index. Differences in the index mean values between the ring-barked and control group were not significant ($p > .05$) for all five indices. Significance means the chance, that differences between the tested groups occur randomly. In this case the t-test results imply, that all observed differences in index mean values between the ring-barked and control group occur randomly in sample IV . Although differences between those groups were observed in sample I , II and III (see appendix C.1).

Table 6.10 displays the independent samples t-test results for age class 1 from sample I to sample IV to check if differences in mean index values between the ring-barked and control group occur mainly in sample IV .

Table 6.10.: T-test results for differences between mean index values of 'ring-barked' and 'control' group for age class 1 in sample I to sample IV with n.s. = not significant

	Age class 1 - Sample 1	Age class 1 - Sample 2	Age class 1 - Sample 3	Age class 1 - Sample 4
NDVI	$t(254) = 2.383, p \leq 0.05$	$t(254) = 1.024, n.s.$	$t(254) = -0.651, n.s.$	$t(254) = 1.703, n.s.$
RENDVI	$t(254) = 6.681, p \leq 0.05$	$t(254) = 0.358, n.s.$	$t(254) = -1.289, n.s.$	$t(254) = -2.785, p \leq 0.05$
NDWI	$t(254) = 1.792, n.s.$	$t(254) = -2.946, p \leq 0.05$	$t(254) = -2.503, p \leq 0.05$	$t(254) = -1.319, n.s.$
NDLI	$t(254) = 0.924, n.s.$	$t(254) = -0.282, n.s.$	$t(254) = -1.343, n.s.$	$t(254) = -2.251, p \leq 0.05$
PSRI	$t(254) = 1.071, n.s.$	$t(254) = 4.622, p \leq 0.05$	$t(254) = 2.663, p \leq 0.05$	$t(254) = 5.004, p \leq 0.05$

It is displayed in table 6.10 that significant differences between ring-barked and control trees occur in all four samples in different indices. Following the interpretation of t-test results it means that in sample 1 differences in mean index values between ring-barked and control trees of NDVI and RENDVI are not randomly. The same applies to the NDWI and the PSRI index values in sample II and III and the RENDWI, NDLI and the PSRI index values in sample IV . On the whole this table does not show any trend which clearly leads to a differentiation of ring-barked and control trees with mean index value comparison.

The same can be observed for sample two (see appendix C.2.2).

7. Discussion and outlook

Based on knowledge acquired during this work, this chapter discusses the results and how they can be interpreted. It will be explained why it is possible that no changes occur within the needle spectra and which plant-physiological background could lead to this. Finally an outlook will be given for further research which is necessary to bring out advantages of hyperspectral remote sensing in early detection of forest health changes.

7.1. Analysis of results

First of all, the results are summarized before they are interpreted on plant-physiological level.

7.1.1. Discrimination of ring-barked group from control group

An early identification of weakened trees might be an important tool for foresters to minimize economical and biological loss due to insect infestations, especially bark-beetle calamities. The sooner changes in the health status of a forest stand can be detected, the faster forest managers can take countermeasures and the more effective they can be.

Spectra of ring-barked and control trees The first goal was to distinguish ring-barked trees from unaffected control trees by detecting changes in their needle reflectance spectra. For that reason needle samples of ring-barked and control trees were taken four times and measured in the spectral laboratory of the DLR Oberpfaffenhofen Earth Observatory Center. As expected these reflectance spectra appeared similar. All trees were still green when the fourth sample was taken in November and due to that all spectra show the characteristic chlorophyll absorption features. On first sight, it was not possible to distinguish visually between ring-barked and control trees (see figure 6.1). The third age class showed some discoloration, but this was observable in both groups, ring-barked and control, alike. Figure 6.2 shows the reflectance spectra of a healthy and a discolored age class. This shows, that it is generally possible to detect discoloration with the reflectance spectra.

Spectra discrimination The first two PCAs were calculated for reflectance spectra of needle samples as well as for their first and second derivative. Different studies show that it is possible to use this method for a distinction between species (Pinnel, 2007; Holden & LeDrew, 1998). It was possible to distinguish between age classes

(see figure 6.3), especially the first and second against the third and fourth age classes, on the other hand no distinction between ring-barked and control trees was possible. Neither a PCA of single samples (see figure 6.4) nor a PCA for single age classes (see figure 6.5) showed a differentiation possibility between ring-barked and control trees. The same applies to the PCA results for the first (see section 6.2) and second derivative (see appendix A.2) of the reflectance spectra. The first two principal components of the reflectance spectra proved unsuitable to distinguish between the ring-barked and control group, neither with the first nor with the second derivative (see subsection 6.2.2 and appendix A.2).

Furthermore the Jeffries-Matusita distance was calculated. The JM distance is a distance measure which can be used to determine species separation (Pinnel, 2007). It was calculated to find out how well ring-barked and control trees can be distinguished within one age class and per sample. The JM distance did not show a significant differentiation possibility between ring-barked and control trees neither for reflectance spectra nor for their derivatives.

In addition to the PCA and the JM distance several health related indices were calculated. Neither of them showed a differentiation possibility between the ring-barked and control trees. According to Campbell *et al.* (2004) it is possible to detect initial damage in Norway spruce canopies with indices, mainly in the 673 to 724 nm spectral region. All chosen indices yielded values within their respective range for green and healthy vegetation (see table 6.7). Furthermore, index mean values were compared with the t-test for mean comparison. Table 6.9 shows the results for the unpaired sample t-test between the ring-barked and control treesfor each index. No significant difference between the groups was indicated. It can be concluded that ring-barking had no significant influence on the index mean values. Additionally the t-test was applied per age class. Table 6.10 shows that differences occur between both groups. They already occur in the first sample in the beginning and they fluctuate from sample to sample. Similar effects were observed for all four age classes (see appendix C.2). It was not possible to detect any trend with the index data and mean value comparison.

In summary it was not possible to distinguish between ring-barked and control trees with either first two principal components of the reflectance and derivative spectra, JM distance or indices and index mean-comparison. The first hypothesis that it would be possible to distinguish optically between healthy and damaged trees after a time period of five months is rejected. Due to this result it is not possible to verify or reject the two other hypotheses. Even though other studies suggest that it is possible to detect changes Buschmann *et al.* (1991); Campbell *et al.* (2004); Mohammed *et al.*

(2000); Sampson *et al.* (2003), in this case no changes were detected with any of the available methods, so the only conclusion is, that no detectable changes occurred within the time-frame of the experiment.

7.1.2. Plant-physiological interpretation of results

After rejecting the first hypothesis that it is possible to distinguish between healthy and damaged trees after five month optically the other two hypotheses remain unanswered. Without changes in needle colors it is not possible to define a point in time were the change is detectable or to prove whether the applied methodology is appropriate for change detection. At this point it is necessary to take a closer look at the underlying physiological processes. There are different scenarios which may lead to no differentiation possibilities between the ring-barked and the control group. The simplest possibility would be that the methodology chosen was not appropriate for early detection of changes in the reflectance spectra. On the other hand these methods were already successfully used for change detection and differentiation as described in section 3.3 and a variety of methods using different approaches were applied, so this possibility is considered unlikely. The other more complex scenario would be, that the method of simulating damage that was used, did not cause any detectable changes after a time period of five months.

Interruption of assimilate transportation and its impacts For better understanding it is necessary to take a closer look at the experimental set-up and the impacts of ring-barking on water- and assimilate cycles. The assimilate and water transportation system was already described in section 3.2. If this cycle is interrupted the effects depend on the location of the interruption and the affected parts of the transportation system. For example an interruption of water supply due to drought, soil acidification or root damage would lead to higher transpiration rates than water can be absorbed by the root system. As a result of constant water shortage needles change their color from green to brown and if the water transport is completely interrupted the whole tree is dying off. How fast the tree shows symptoms depends on the species and its liability for water stress. Another example for disruption of water- and assimilate cycle is a severe bark-beetle infestation. In spruce stands *Pityogenes chalcographus* and *Ips typographus* cause most damages. Both beetles are phloeophag which means they live on the bast layer which includes the phloem. Depending on the strength of the infestation the assimilate transportation is completely or partially interrupted and the interruption can occur at different heights of the trunk. This again leads to different symptoms. The higher the interruption of the assimilate transportation on the trunk occurs, the faster an

accumulation of assimilates in the needles leads to premature senescence (Majunke, 2013). Finally, it is important to mention that in context with heavy bark-beetle infestations a typical change in needle color of spruce trees begins from the lower part of the crown. This is a symptom which can be explained due to the fact that assimilates produced by lower levels in the crown are mainly transported to the root system (Raven *et al.*, 2006) and due to this these parts are the first to be affected by the interruption. A more detailed description about physiological processes during accumulation of photosynthetic products in leaves and the feedback reaction can be read in the paper 'Sink regulation of photosynthesis' by Paul & Foyer (2001).

In case of this experiment the assimilate transportation flow to the root system was interrupted at breast height diameter, 1.30 m above ground. Physiologically it leads to abortion of carbohydrates supply of the root system like a bark-beetle infestation would do, but on a very low level of the trunk. Typically Norway spruce trees of the examined age at these stands have a height of around 25 to 30 meters, thus a long pipeline in which assimilates can be accumulated before they remain in the needles in a critical concentration. Due to this, expected changes due to assimilate accumulation in needles and the subsequent senescence, which would happen in case of heavy bark-beetle infestations, do not occur. Changes which can be expected will more likely occur due to carbohydrate under-supply of the root system and the following pathology. These alterations will take time due to assimilate storage which is supported by ring-barking experiments of Roth *et al.* (2001). The time delay until the root system is affected by the interrupted assimilate flow is furthermore supported by Lösch (2003). He describes that root and shoot growth are in dynamic interaction with each other and roots are mainly growing and thus using photosynthesis product,s during spring and autumn.

7.2. Methodology evaluation

Both the JM distance and the indices were applied to bands of the reflectance spectra which are often related to the health status of vegetation.

Laengere Zeitspanne zwischen der schaedigung und den symptomen verweise auf dieses kapitel im naechstn Bands in the visible range, which were described to be very sensitive to initial damage (Campbell *et al.*, 2004) and channels in the infrared range which include lignin and water absorption bands. Although, chosen bands are narrow in case of hyperspectral data, it was not possible to discover differences between the ring-barked and control group.

7.3. Experimental set-up evaluation

The experimental set-up was planned to imitate a bark-beetle attack. For this purpose, trees were ring-barked to interrupt their carbohydrate transport system. As ring-barking was conducted at a height of 1.30 m above ground the plant physiological effects are different than what was initially sought for. This kind of intervention in the assimilate transportation flow leads to a much longer time period between damage and upcoming symptoms in the crowns of damaged trees as described in section 7.2. In this study a time span of five months during the vegetation period was too short for detectable symptoms to take place.

In case of heavy real-life bark-beetle attacks the time period between damage and symptom can be much shorter. Experience shows that trees which are heavily affected by bark-beetles show symptoms within a few months . Ring-barking is good for initial determination of the possibility to detect changes within the spectrum of green needles, due to damages. Finally needle samples need to be collected over a longer time period than five months to observe first changes with this weakening method.

If a faster change in the behavior of trees should be simulated, another method needs to be developed. Ring-barking could be improved in effectiveness to also affect water flow from the root system to the crown. Therefore the last annual growth rings needs to be cut as well. Following the idea of simulation of bark beetle attacks, ring-barking should be conducted much higher than 1.30 m above ground. With that the assimilate accumulation in needles can be accelerated similarly to bark-beetle infestations.

7.4. Outlook

The time series is continued in 2014. Further needle sampling is planned as well as airborne data takes. Additionally a method comparison of needle spectra measurements is scheduled to be conducted, to determine differences between laboratory and field measurements. This is necessary to develop a reliable method for needle reflectance spectra measurements at leaf level.

Early detection of changes in the health status of vegetation with airborne data is a very complex matter due to various factors which play a role. There is vitality, water supply, location, intensity and type of damage. Additionally, due to storage substances trees might react with delay to damages. This leads to a huge variability concerning the time frame between damage and first signs of damage.

Concerning needle reflectance spectra, the time frame between reflectance spectrum changes and needle color fading needs to be examined. It is of interest if needle reflectance spectra show changes earlier if a tree is non vital in comparison to a vital tree. In this context it needs to be determined if needle reflectance spectra of healthy, vital trees have the same reflectance spectrum like needles of non vital trees.

After determination of plant physiological behavior and reflectance spectra changes in the laboratory it is important to review how to use it at canopy scale with air- or spaceborn remote. Due to coarser resolutions of these, changes might be detectable later.

A particular challenge in remote sensing of forest stands health status is, that it needs to be evaluated in comparison to other forest stands of the same age with the same stand conditions. In case of Bavaria where most of the Norway spruce stands are not natural and grow under unfavorable circumstances (see section 3.1) this might become a problem.

Finally it needs to be determined if ‘early ‘in remote sensing is early enough for countermeasures.

8. Conclusion

It was not possible to distinguish between artificially weakened trees and unaffected control trees after five month. Ring-barking of Norway spruce trees at a height of around 1.30 m did not lead to changes in the reflectance spectra which can be detected with the chosen methodology. Most likely due to the physiological behavior of Norway spruce trees. The experimental set-up allows for a slow decline in health status and with that a wide time frame for needle reflectance spectra change detection. The experiment shows that it can take more than five months from the damaging event to detectable symptoms in green needles showing. This time frame might be much shorter in cases of different damages to the tree regarding location and severity. With that it can be said that 'early detection' is a broad term in context with forest health monitoring, which strongly depends on location, kind and severity of damage as well as environmental circumstances.

References

ASD Inc. 2013. *ASD inc. [ONLINE].*

Bayer, Anita. 2013. *Methodological Developments for Mapping Soil Constituents using Imaging Spectroscopy.* Dissertation, Universität Potsdam.

Bayerische Landesanstalt für Wald und Forstwirtschaft (LWF). 2009. *Fichtenwälder im Klimawandel - Wissen 63.* Tech. rept. Bayrische Landesanstalt für Wald und Forstwirtschaft (LWF), Freising.

Bayerische Staatsforsten. 2013. *Forstbetrieb Wasserburg an der Inn - Exkursionsführer.*

Bayerisches Landesamt für Umwelt. 2014. *Potentielle Natürliche Vegetation (PNV) Bayern [Online].* http://www.lfu.bayern.de/natur/potentielle_natuerliche_vegetation/index.htm [Accessed 25 February 2014].

Beck, Erwin H, Fettig, Sebastian, Knake, Claudia, Hartig, Katja, & Bhattarai, Tribikram. 2007. Specific and unspecific responses of plants to cold and drought stress. *Journal of Biosciences*, **32**(April), 501–510.

Boa, Eric. 2003. *An illustrated guide to the state of health of trees. Recognition and interpretation.* Tech. rept. Food and Agriculture Organization of the United Nations, Egham, Surrey, United Kingdom.

Bortz, J. 1989. *Statistik: f{ü}r Sozialwissenschaftler.* Springer-Lehrbuch. Springer-Verlag.

Bundesministerium für Ernährung, Landwirtschaft und Verbraucherschutz. 2004. *Bundeswaldinventur 2.* http://www.bundeswaldinventur.de [Accessed: 4th December 2013].

Bundesministerium für Ernährung, Landwirtschaft und Verbraucherschutz. 2011. *German forests - Nature and economic factor.* Tech. rept. Bundesministerium für Ernährung, Landwirtschaft und Verbraucherschutz.

Bundesministerium für Ernährung, Landwirtschaft und Verbraucherschutz. 2012. *Ergebnisse der Waldzustandserhebung 2012.* Tech. rept. Bundesministerium für Ernährung, Landwirtschaft und Verbraucherschutz.

Buschmann, Claus. 1993. Fernerkundung von Pflanzen. *Naturwissenschaften*, **80**, 439–453.

Buschmann, Claus, Rinderle, Ursula, & Lichtenthaler, Hartmut K. 1991. Detection of stress in coniferous forest trees with the VIRAF spectrometer. *Geoscience and Remote Sensing*, **29**(1), 96–100.

Campbell, P. K. Entcheva, Rock, B. N., Martin, M. E., Neefus, C. D., Irons, J. R., Middleton, E. M., & Albrechtova, J. 2004. Detection of initial damage in Norway spruce canopies using hyperspectral airborne data. *International Journal of Remote Sensing*, **25**(24), 5557–5584.

Ceccato, Pietro, Gobron, Nadine, Flasse, Stéphane, Pinty, Bernard, & Tarantola, Stefano. 2002a. Designing a spectral index to estimate vegetation water content from remote sensing data : Part 1 Theoretical approach. *Remote Sensing of Environment*, **82**, 188–197.

Ceccato, Pietro, Flasse, Stéphane, & Grégoire, Jean-Marie. 2002b. Designing a spectral index to estimate vegetation water content from remote sensing data Part 2 . Validation and applications. *Remote Sensing of Environment*, **82**, 198–207.

Chen, J M, & Black, T A. 1992. Defining leaf area index for non-flat leaves. *Plant, Cell and Environment*, **15**, 421–429.

Chen, J M, & Cihlar, J. 1996. Retrieving leaf area index of boreal conifer forests using landsat TM images. *Remote Sensing of Environment*, **55**(2), 153–162.

Clark, Roger N, King, Trude V V, Ager, Cathy, & Swayze, Gregg A. 1993. Initial Vegetation Species and Senescence/Stress Indicator Mapping in the San Luis Valley, Colorado Using Imaging Spectrometer Data. *Colorado Geological Survey Special Publication*, **38**, 35–38.

Damm, Alexander. 2008. *Hyperspektrale Fernerkundung zur Ableitung pflanzenphysiologischer Parameter von Stadtbäumen - Strahlungstransfermodellierung für Berliner Kastanienbestände.* Ph.D. thesis, Humboldt-Universität zu Berlin - Geographisches Institut.

Delegido, J, Verrelst, J, Meza, C M, Rivera, J P, Alonso, L, & Moreno, J. 2013. A red-edge spectral index for remote sensing estimation of green LAI over agroecosystems. *European Journal of Agronomy*, **46**, 42–52.

Eastman, J R, Sangermano, F, Machado, E A, Rogan, J, & Anyamba, A. 2013. Global trends in seasonality of Normalized Difference Vegetation Index (NDVI), 1982-2011. *Remote Sensing*, **5**(10), 4799–4818.

Food and Agriculture Organization of the United States. 2010. *Global Forest Resources Assessment 2010*. Tech. rept. Food and Agriculture Organization of the United States, Rome.

Freitag, Winfried. 2013. *Historisches Lexikon Bayerns*. http://www.historisches-lexikon-bayerns.de/artikel/artikel_45651#17 [Accessed 3 December 2013].

Gamon, A, Peñuelas, J, & Field, C B. 1992. A Narrow-Waveband Spectral Index That Tracks Diurnal Changes in Photosynthetic Efficiency. *Remote Sensing of Environment*, **41**, 35–44.

Gao, BC. 1996. NDWI - a normalized difference water index for remote sensing of vegetation liquid water from space. *Remote sensing of environment*, **266**(April 1995), 257–266.

Gao, BC, & Goetz, AFH. 1994. Extraction of dry leaf spectral features from reflectance spectra of green vegetation. *Remote Sensing of Environment*, **374**(June 1993), 369–374.

Gitelson, a a, Merzlyak, M N, & Chivkunova, O B. 2001. Optical properties and nondestructive estimation of anthocyanin content in plant leaves. *Photochemistry and photobiology*, **74**(1), 38–45.

Gitelson, Anatoly, & Merzlyak, Mark N. 1994. Spectral Reflectance Changes Associated with Autumn Senescence of Aesculus hippocastanum L. and Acer platanoides L. Leaves. Spectral Features and Relation to Chlorophyll Estimation. *Journal of Plant Physiology*, **143**(3), 286–292.

Gitelson, Anatoly A. 2012. Remote Sensing Estimation of Crop Biophysical Characteristics at Various Scales. *Chap. 15, pages 329–358 of:* Thenkabail, Prasad S., Lyon, John G., & Huete, Alfredo (eds), *Hyperspectral Remote Sensing of Vegetation*. Taylor&Francis Group.

Gitelson, Anatoly a, Zur, Yoav, Chivkunova, Olga B, & Merzlyak, Mark N. 2002. Assessing carotenoid content in plant leaves with reflectance spectroscopy. *Photochemistry and photobiology*, **75**(3), 272–281.

Guiard, V., & Rasch, D. 2004. The Robustness of two sample tests for Means - A Reply on von Eye's Comment. *Psychology Science*, **46**(4), 549–553.

Helms, J A. 1998. *The Dictionary of Forestry.* Society of American Foresters and CABI Pub.

Herrmann, I, Karnieli, A, Bonfil, D J, Cohen, Y, & Alchantis, V. 2010. SWIR-based spectral indices for assessing nitrogen content in potato fields. *International Journal of Remote Sensing*, **31**(19), 5127–5143.

Holden, H, & LeDrew, E. 1998. Spectral Discrimination of Healthy and Non-Healthy Corals Based on Cluster Analysis , Principal Components Analysis , and Derivative Spectroscopy. *Remote sensing of environment*, **65**(February), 217–224.

Huete, A R, Liu, H Q, Batchily, K, & Leeuwen, W Van. 1997. A Comparison of Vegetation Indices over a Global Set of TM Images for EOS-MODIS. *Remote sensing of environment*, **59**, 440–451.

Hunt, E Raymond, & Yilmaz, M Tugrul. 2007. Remote Sensing of Vegetation Water Content using Shortwave Infrared Reflectances. *Proceedings of SPIE*, **6679**(1), 1–8.

Hunt, E Raymond, Li, Li, Yilmaz, M Tugrul, & Jackson, Thomas J. 2011. Comparison of vegetation water contents derived from shortwave-infrared and passive-microwave sensors over central Iowa. *Remote Sensing of Environment*, 1–19.

Jackson, T. J. 2004. Vegetation water content mapping using Landsat data derived normalized difference water index for corn and soybeans. *Remote Sensing of Environment*, **92**(4), 475–482.

Jonckheere, I., Muys, B., & Coppin, P. 2005. Derivative analysis for in situ high dynmaic range hemispherical photography and its application in forest stands. *IEEE Geoscience and Remote Sensing Letters*, **2**(3), 296–300.

Jones, H G, & Vaughan, R A. 2010. *Remote sensing of vegetation: principles, techniques, and applications.* Oxford University Press.

Klug, Peter. 2005. Vitalität und Entwicklungsphasen bei Bäumen. *ProBaum*, **1**, 1–4.

Larcher, Walter. 1987. Stress bei Pflanzen. *Naturwissenschaften*, **74**, 158–167.

Larcher, Walter. 2001. *Ökophysiologie der Pflanzen: Leben, Leistung und Streßbewältigung der Pflanzen in ihrer Umwelt.* UTB f{ü}r Wissenschaft. Ulmer.

Lausch, a., Heurich, M., Gordalla, D., Dobner, H.-J., Gwillym-Margianto, S., & Salbach, C. 2013. Forecasting potential bark beetle outbreaks based on spruce forest vitality using hyperspectral remote-sensing techniques at different scales. *Forest Ecology and Management*, **308**(Nov.), 76–89.

Lichtenthaler, Hartmut K. 1996. Vegetation Stress: an Introduction to the Stress Concept in Plants. *Journal of Plant Physiology*, **148**(1-2), 4–14.

Lillesand, T M, Kiefer, R W, & Chipman, J W. 2004. *Remote Sensing and Image Interpretation.* John Wiley & Sons Canada, Limited.

Lösch, Rainer. 2003. *Wasserhaushalt der Pflanzen.* 2 edn. Quelle & Meyer Verlag.

Majunke, C. 2013. *Personal communication.*

Merzlyak, Mark N., & Gitelson, Anatoly. 1995. Why and What for the Leaves Are Yellow in Autumn? On the Interpretation of Optical Spectra of Senescing Leaves (Acerplatanoides L.). *Journal of Plant Physiology*, **145**(3), 315–320.

Merzlyak, Mark N, Gitelson, Anatoly A, Chivkunova, Olga B, Yu, Victor, & Campus, Sede Boker. 1999. Non-destructive optical detection of pigment changes during leaf senescence and fruit ripening. *Physiologia Plantarum*, **106**, 135–141.

Mohammed, Gina H., Noland, Thomas L., Sampson, Paul H, Zarco-tejada, Pablo J, Irving, Denzil, & Miller, John R. 2000. *Natural and stress-induced effects on leaf spectral reflectance in Ontario species.* Tech. rept. Ontario Forest Research Institute, Ontario.

National Aeronautics and Space Administration (NASA). 2014. *Global Change Master Directory [ONLINE].* http://gcmd.nasa.gov/records/GCMD_GLCF_GIMMS.html [Accessed 29 January 2013].

Norsk Elektronik Optikk. 2013. *HySpex - High resolution, high speed hyperspectral cameras for laboratory, industrial and airborne applications.*

O'Laughlin, Jay, Livingston, R Ladd, Thier, Ralph, Thornton, John P, Toweill, Dale E, & Morelan, Lyn. 1994. Defining and Measuring Forest Health. *Journal of Sustainable Forestry*, **2**(1-2), 65–85.

Pate, J.S. 1975. Exchange of solutes between phloem and xylem and circulation in the whole plant. *Chap. 19 of:* Zimmermann, M.H., & Milburn, J.A. (eds), *Transport in Plants I - Phloem Transport.* Berlin: Springer-Verlag.

Paul, M J, & Foyer, C H. 2001. Sink regulation of photosynthesis. *Journal of experimental botany*, **52**(360), 1383–400.

Peñuelas, J, Baret, F, & Filella, I. 1995. Semi-empirical indices to assess carotenoids/chlorophyll a ratio from leaf spectral reflectances. *Photosynthetica*, **31**.

Pinnel, Nicole. 2007. *A method for mapping submerged macrophytes in lakes using hyperspectral remote sensing.* Ph.D. thesis, Technische Universität München.

Puhe, Joachim. 2003. Growth and development of the root system of Norway spruce (Picea abies) in forest stands - a review. *Forest Ecology and Management*, **175**, 253–273.

Rautiainen, Miina. 2005. *The spectral signature of coniferous forests: the role of stand structure and leaf area index.* Ph.D. thesis, University of Helsinki.

Raven, P H, Evert, R F, & Eichhorn, S E. 2006. *Biologie der Pflanzen.* de Gruyter.

Resa, F. 1877. *Ueber die Periode der Wurzelbildung.* Carthaus.

Richards, J A, & Jia, X. 2006. *Remote Sensing Digital Image Analysis: An Introduction.* Springer.

Roberts, D.a., Smith, M.O., & Adams, J.B. 1993. Green vegetation, nonphotosynthetic vegetation, and soils in AVIRIS data. *Remote Sensing of Environment*, **44**(2-3), 255–269.

Roth, Bernhard, Bucher, Hans-Ulrich, Schütz, Jean-Philippe, & Ammann, Peter. 2001. Ringeln - Alte Methode neu angwendet. *Wald Und Holz*, **4**, 38–41.

Sampson, Paul H., Zarco-Tejada, Pablo J., Mohammed, Gina H., Miller, John R., & Noland, Thomas L. 2003. Hyperspectral Remote Sensing of Forest Condition: Estimating Chlorophyll Content in Tolerant Hardwoods. *Forest Science*, **49**(3), 381–391.

Savitzky, Abraham, & Golay, Marcel J. E. 1964. Smootihing and Differentiation of Data by Simplified Leas Square Procedures. *Analytical Chemistry*, **36**(8), 1627–1639.

Schäfer, Roland. 2001. *Lamettasyndrom und Säuresteppe: Das Waldsterben und die Forstwissenschaft 1979-2007.* Ph.D. thesis, Albert-Ludwigs-Universität Freiburg.

Schopfer, P, & Axel, B. 2010. *Pflanzenphysiologie.* Spektrum Akademischer Verlag GmbH.

Sellers, P.J. 1985. International Journal of Remote Sensing Canopy reflectance , photosynthesis and transpiration. *International Journal of Remote Sensing*, **6**(8), 1335–1372.

Sepulcre-Cantó, G., Zarco-Tejada, P.J., Jiménez-Muñoz, J.C., Sobrino, J.a., Miguel, E. De, & Villalobos, F.J. 2006. Detection of water stress in an olive orchard with thermal remote sensing imagery. *Agricultural and Forest Meteorology*, **136**(1-2), 31–44.

Serrano, Lydia, Peñuelas, Josep, & Ustin, Susan L. 2002. Remote sensing of nitrogen and lignin in Mediterranean vegetation from AVIRIS data: Decomposing biochemical from structural signals. *Remote Sensing of Environment*, **81**, 355–364.

Shigo, A L. 1994. *Moderne Baumpflege: Grundlagen der Baumbiologie.* Thalacker Verlag.

Sims, Daniel A, & Gamon, John A. 2002. Relationships between leaf pigment content and spectral reflectance across a wide range of species, leaf structures and developmental stages. *Remote Sensing of Environment*, **81**(2-3), 337–354.

Tsai, Fuan, & Philpot, William. 1998. Derivative Analysis of Hyperspectral Data. *Remote Sensing of Environment*, **66**(1), 41–51.

Vollenweider, P, & Günthardt-Goerg, MS. 2005. Diagnosis of abiotic and biotic stress factors using the visible symptoms in foliage. *Environmental Pollution*, **137**, 455–465.

Wessman, Carol A, Aber, John D, Peterson, David L, & Melillo, Jerry M. 1988. Remote sensing of canopy chemistry and nitrogen cycling in temperate forest ecosystems. *Nature*, **355**, 154–156.

Yi, K, Tani, H, Zhang, J, Guo, M, Wang, X, & Zhong, G. 2013. Long-term satellite detection of post-fire vegetation trends in boreal forests of China. *Remote Sensing*, **5**(12), 6938–6957.

Zang, Christian, Rothe, Andreas, Weis, Wendelin, & Pretzsch, Hans. 2011. Zur Baumarteneignung bei Klimawandel: Ableitung der Trockenstress - Anfälligkeit wichtiger Waldbaumarten aus Jahrringbreiten. *Allgemeine Forst und Jagdzeitung*, **182**, 98–112.

Zhang, Y, Qi, W, Zhou, C, Ding, M, Liu, L, Gao, J, Bai, W, Wang, Z, & Zheng, D. 2014. Spatial and temporal variability in the net primary production of alpine grassland on the Tibetan Plateau since 1982. *Journal of Geographical Sciences*, **24**(2), 269–287.

A. PCA results

A.1. PCA results for reflectance spectra of sample two and three

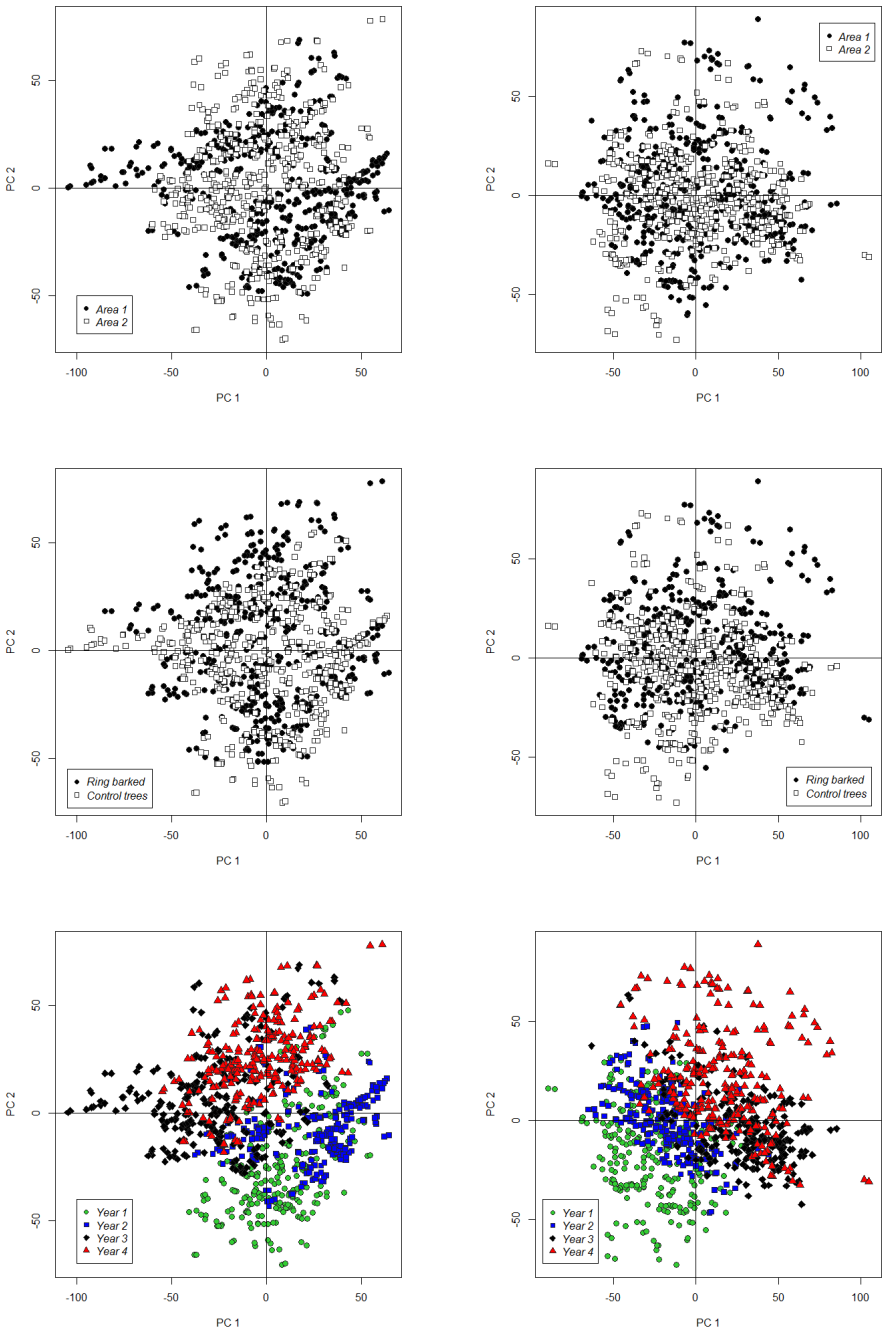

Figure A.1.: Principle component analysis for sample two (Left side) and sample three (Right side), split by area (Top), ring barked and control trees (Middle) and age class (Bottom)

A.2. PCA results for derivative two

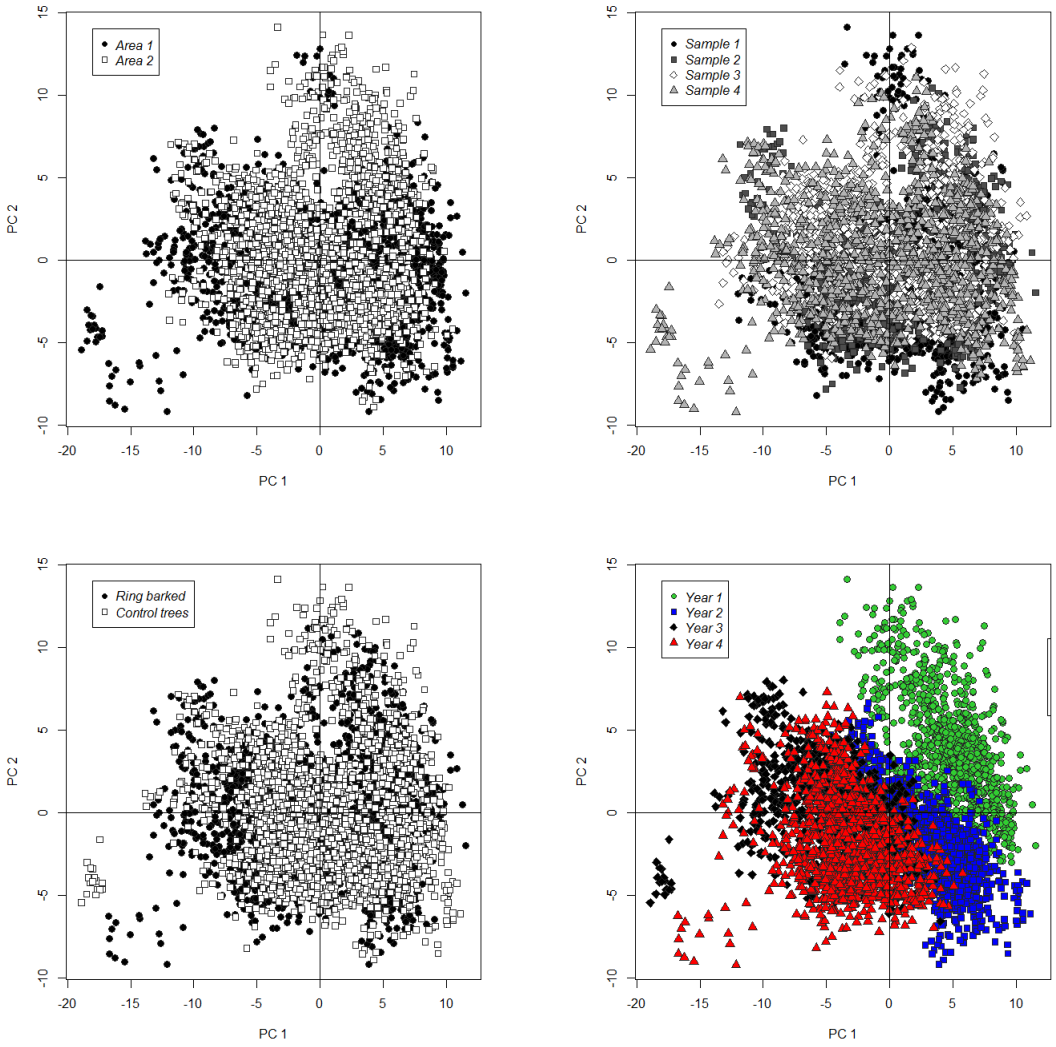

Figure A.2.: Principle component analysis for 2^{nd} derivative of all reflectance spectra split by experimental side (Top left), by sample (Top right), by ring barked and control trees (Bottom left) and by age class (Bottom right)

B. Jeffries-Matusita Distance Tables

B.1. JM distance for spectra

Table B.1.: Jeffries-Matusita Distance for sample 2, splitted by year with the bands 600, 650, 705, 750, 1241 and 1754 nm

	1r	1c	2r	2c	3r	3c	4r	4c
1r		**0.86**	1.50	1.79	1.98	1.96	1.97	1.95
1c	0.56		1.79	1.96	2.00	2.00	1.99	2.00
2r	1.39	2.25		**0.96**	1.79	1.75	1.85	1.63
2c	2.26	3.89	0.66		1.97	1.96	2.00	1.93
3r	4.58	8.98	2.27	4.21		**1.21**	1.08	1.44
3c	3.94	10.51	2.06	3.88	0.93		1.67	1.54
4r	4.15	5.77	2.60	6.41	0.78	1.80		**1.03**
4c	3.60	7.13	1.69	3.33	1.27	1.47	0.72	

Table B.2.: Jeffries-Matusita Distance for sample 3, splitted by year with the bands 600, 650, 705, 750, 1241 and 1754 nm

	1r	1c	2r	2c	3r	3c	4r	4c
1r		**0.84**	1.81	1.88	1.97	1.95	1.99	1.97
1c	0.54		1.80	1.84	2.00	2.00	1.97	1.99
2r	2.37	2.29		**0.94**	2.00	1.99	1.92	1.99
2c	2.85	2.51	0.63		2.00	1.94	1.92	1.98
3r	4.27	7.00	8.33	6.67		**1.43**	1.14	1.49
3c	3.62	7.65	5.33	3.47	1.26		1.78	1.39
4r	5.08	4.37	3.19	3.22	0.84	2.19		**1.26**
4c	4.14	5.34	5.39	4.38	1.36	1.19	0.99	

B.2. JM distance for 1st derivative of spectra

Table B.3.: Jeffries-Matusita Distance for derivative 1 of sample 2, splitted by year with the bands 600, 650, 705, 750, 1241 and 1754 nm. The upper right side shows the Jeffries-Matusita distance, the lower left side shows the Bhattacharyya Index

	1r	1c	2r	2c	3r	3c	4r	4c
1r		**0.25**	0.99	1.11	0.95	1.06	1.04	1.19
1c	0.13		1.26	1.32	1.30	1.33	1.40	1.48
2r	0.69	0.99		**0.28**	0.50	0.47	0.63	0.44
2c	0.80	1.08	0.15		0.73	0.31	0.82	0.60
3r	0.65	1.05	0.28	0.46		**0.62**	0.39	0.56
3c	0.75	1.09	0.26	0.17	0.37		0.80	0.66
4r	0.73	1.20	0.38	0.53	0.22	0.51		**0.37**
4c	0.90	1.35	0.25	0.36	0.33	0.40	0.21	

Table B.4.: Jeffries-Matusita Distance for derivative 1 of sample 3, splitted by year with the bands 600, 650, 705, 750, 1241 and 1754 nm. The upper right side shows the Jeffries-Matusita distance, the lower left side shows the Bhattacharyya Index

	1r	1c	2r	2c	3r	3c	4r	4c
1r		**0.26**	1.16	1.19	1.04	0.88	1.35	1.05
1c	0.14		1.17	1.19	1.17	1.01	1.33	1.11
2r	0.87	0.88		**0.20**	0.50	0.47	0.54	0.61
2c	0.90	0.91	0.10		0.51	0.54	0.54	0.63
3r	0.74	0.89	0.29	0.30		**0.48**	0.74	0.67
3c	0.58	0.70	0.27	0.32	0.28		0.78	0.75
4r	1.13	1.09	0.31	0.31	0.47	0.49		**0.29**
4c	0.74	0.81	0.37	0.38	0.41	0.47	0.16	

B.3. JM distance for 2nd derivative of spectra

Table B.5.: Jeffries-Matusita Distance for derivative 2 of sample 2, splitted by year with the bands 600, 650, 705, 750, 1241 and 1754 nm. The upper right side shows the Jeffries-Matusita distance, the lower left side shows the Bhattacharyya Index

	1r	1c	2r	2c	3r	3c	4r	4c
1r		**0.17**	0.42	0.32	0.38	0.34	0.24	0.20
1c	0.09		0.55	0.35	0.24	0.18	0.25	0.24
2r	0.24	0.32		**0.12**	0.65	0.46	0.58	0.49
2c	0.18	0.19	0.06		0.45	0.28	0.41	0.32
3r	0.21	0.13	0.40	0.25		**0.12**	0.19	0.26
3c	0.19	0.09	0.26	0.15	0.06		0.18	0.21
4r	0.13	0.13	0.34	0.23	0.10	0.10		**0.19**
4c	0.11	0.13	0.28	0.18	0.14	0.11	0.10	

Table B.6.: Jeffries-Matusita Distance for derivative 2 of sample 3, splitted by year with the bands 600, 650, 705, 750, 1241 and 1754 nm. The upper right side shows the Jeffries-Matusita distance, the lower left side shows the Bhattacharyya Index

	1r	1c	2r	2c	3r	3c	4r	4c
1r		**0.08**	0.35	0.29	0.35	0.25	0.46	0.31
1c	0.04		0.34	0.28	0.36	0.28	0.49	0.38
2r	0.19	0.19		**0.14**	0.59	0.49	0.90	0.79
2c	0.16	0.15	0.07		0.63	0.53	0.88	0.77
3r	0.19	0.20	0.35	0.38		**0.09**	0.26	0.32
3c	0.13	0.15	0.28	0.31	0.05		0.21	0.27
4r	0.26	0.28	0.60	0.58	0.14	0.11		**0.16**
4c	0.17	0.21	0.50	0.49	0.18	0.14	0.08	

C. SPSS Outputs

C.1. SPSS output tables for the independent samples t-test per sample between the ring-barked and control group.

Sample 1

	ring_barked	H	Mittelwert	Standardabweichung	Standardfehler Mittelwert
NDLI	1	504	,04769	,003693	,000165
	2	504	,04817	,003224	,000144
RENDVI	1	504	,5621	,03526	,00157
	2	504	,5618	,03574	,00159
NDWI	1	504	,0819	,03864	,00172
	2	504	,0893	,03210	,00143
PSRI	1	504	-,0101	,00703	,00031
	2	504	-,0115	,00896	,00040
NDVI	1	504	,8494	,02134	,00095
	2	504	,8493	,01950	,00087

Test bei unabhängigen Stichproben

		Levene-Test der Varianzgleichheit		T-Test für die Mittelwertgleichheit						
									95% Konfidenzintervall der Differenz	
		F	Sig.	t	df	Sig. (2-seitig)	Mittelwert-differenz	Standard-fehlerdifferenz	Unterer	Oberer
NDLI	Varianzgleichheit angenommen	8,828	,003	-2,209	1006	,027	-,000482	,000218	-,000911	-,000054
	Varianzgleichheit nicht angenommen			-2,209	987,982	,027	-,000482	,000218	-,000911	-,000054
RENDVI	Varianzgleichheit angenommen	,139	,709	,174	1006	,862	,00039	,00224	-,00400	,00478
	Varianzgleichheit nicht angenommen			,174	1005,820	,862	,00039	,00224	-,00400	,00478
NDWI	Varianzgleichheit angenommen	39,704	,000	-3,278	1006	,001	-,00734	,00224	-,01173	-,00295
	Varianzgleichheit nicht angenommen			-3,278	973,261	,001	-,00734	,00224	-,01173	-,00295
PSRI	Varianzgleichheit angenommen	3,067	,080	2,640	1006	,008	,00134	,00051	,00034	,00234
	Varianzgleichheit nicht angenommen			2,640	952,180	,008	,00134	,00051	,00034	,00234
NDVI	Varianzgleichheit angenommen	8,949	,003	,111	1006	,912	,00014	,00129	-,00238	,00267
	Varianzgleichheit nicht angenommen			,111	997,957	,912	,00014	,00129	-,00238	,00267

Sample 2

Gruppenstatistik

	ring_barked	H	Mittelwert	Standardabweichung	Standardfehler Mittelwert
RENDVI	1	512	,5503	,04198	,00186
	2	512	,5547	,03868	,00171
NDWI	1	512	,0889	,03588	,00159
	2	512	,0943	,03290	,00145
PSRI	1	512	-,0118	,00628	,00028
	2	512	-,0129	,00701	,00031
NDLI	1	512	,0479	,00324	,00014
	2	512	,0483	,00322	,00014
NDVI	1	512	,8498	,02036	,00090
	2	512	,8495	,02040	,00090

Test bei unabhängigen Stichproben

		Levene-Test der Varianzgleichheit		T-Test für die Mittelwertgleichheit						
									95% Konfidenzintervall der Differenz	
		F	Sig.	t	df	Sig. (2-seitig)	Mittelwertdifferenz	Standardfehlerdifferenz	Unterer	Oberer
RENDVI	Varianzgleichheit angenommen	1,224	,269	-1,748	1022	,081	-,00441	,00252	-,00936	,00054
	Varianzgleichheit nicht angenommen			-1,748	1015,238	,081	-,00441	,00252	-,00936	,00054
NDWI	Varianzgleichheit angenommen	2,421	,120	-2,523	1022	,012	-,00543	,00215	-,00965	-,00121
	Varianzgleichheit nicht angenommen			-2,523	1014,431	,012	-,00543	,00215	-,00965	-,00121
PSRI	Varianzgleichheit angenommen	2,788	,095	2,596	1022	,010	,00108	,00042	,00026	,00190
	Varianzgleichheit nicht angenommen			2,596	1009,698	,010	,00108	,00042	,00026	,00190
NDLI	Varianzgleichheit angenommen	,361	,548	-2,290	1022	,022	-,00046	,00020	-,00086	-,00007
	Varianzgleichheit nicht angenommen			-2,290	1021,948	,022	-,00046	,00020	-,00086	-,00007
NDVI	Varianzgleichheit angenommen	,576	,448	,234	1022	,815	,00030	,00127	-,00220	,00280
	Varianzgleichheit nicht angenommen			,234	1021,996	,815	,00030	,00127	-,00220	,00280

Sample 3

Gruppenstatistik

	ring_barked	H	Mittelwert	Standardabweichung	Standardfehler Mittelwert
RENDVI	1	512	,5363	,04340	,00192
	2	510	,5417	,04210	,00186
NDWI	1	512	,0879	,03636	,00161
	2	510	,0968	,02896	,00128
PSRI	1	512	-,0104	,00705	,00031
	2	510	-,0127	,01084	,00048
NDLI	1	512	,04744	,003711	,000164
	2	510	,04833	,003455	,000153
NDVI	1	512	,8481	,02392	,00106
	2	510	,8468	,02445	,00108

Test bei unabhängigen Stichproben

		Levene-Test der Varianzgleichheit		T-Test für die Mittelwertgleichheit						
									95% Konfidenzintervall der Differenz	
		F	Sig.	t	df	Sig. (2-seitig)	Mittelwertdifferenz	Standardfehlerdifferenz	Unterer	Oberer
RENDVI	Varianzgleichheit angenommen	,065	,799	-2,028	1020	,043	-,00542	,00267	-,01067	-,00018
	Varianzgleichheit nicht angenommen			-2,028	1019,290	,043	-,00542	,00267	-,01067	-,00018
NDWI	Varianzgleichheit angenommen	37,662	,000	-4,342	1020	,000	-,00893	,00206	-,01297	-,00490
	Varianzgleichheit nicht angenommen			-4,344	973,011	,000	-,00893	,00206	-,01297	-,00490
PSRI	Varianzgleichheit angenommen	2,408	,121	3,964	1020	,000	,00227	,00057	,00114	,00339
	Varianzgleichheit nicht angenommen			3,961	873,915	,000	,00227	,00057	,00114	,00339
NDLI	Varianzgleichheit angenommen	4,372	,037	-3,950	1020	,000	-,000886	,000224	-,001326	-,000446
	Varianzgleichheit nicht angenommen			-3,951	1015,371	,000	-,000886	,000224	-,001326	-,000446
NDVI	Varianzgleichheit angenommen	,756	,385	,884	1020	,377	,00134	,00151	-,00163	,00431
	Varianzgleichheit nicht angenommen			,884	1019,333	,377	,00134	,00151	-,00163	,00431

Sample 4

Gruppenstatistik

	ring_barked	H	Mittelwert	Standardabweichung	Standardfehler Mittelwert
RENDVI	1,0	512	,5304	,06204	,00274
	2,0	512	,5306	,07521	,00332
NDWI	1,0	512	,0842	,03889	,00172
	2,0	512	,0887	,03709	,00164
PSRI	1,0	512	,0040	,03530	,00156
	2,0	512	,0013	,03412	,00151
NDLI	1,0	512	,04729	,003275	,000145
	2,0	512	,04738	,003881	,000172
NDVI	1,0	512	,8378	,05417	,00239
	2,0	512	,8330	,06085	,00269

Test bei unabhängigen Stichproben

		Levene-Test der Varianzgleichheit		T-Test für die Mittelwertgleichheit						
									95% Konfidenzintervall der Differenz	
		F	Sig.	t	df	Sig. (2-seitig)	Mittelwertdifferenz	Standardfehlerdifferenz	Unterer	Oberer
RENDVI	Varianzgleichheit angenommen	23,472	,000	-,055	1022	,956	-,00024	,00431	-,00869	,00822
	Varianzgleichheit nicht angenommen			-,055	986,371	,956	-,00024	,00431	-,00869	,00822
NDWI	Varianzgleichheit angenommen	10,793	,001	-1,903	1022	,057	-,00452	,00238	-,00918	,00014
	Varianzgleichheit nicht angenommen			-1,903	1019,719	,057	-,00452	,00238	-,00918	,00014
PSRI	Varianzgleichheit angenommen	,031	,860	1,242	1022	,215	,00269	,00217	-,00156	,00695
	Varianzgleichheit nicht angenommen			1,242	1020,826	,215	,00269	,00217	-,00156	,00695
NDLI	Varianzgleichheit angenommen	12,741	,000	-,380	1022	,704	-,000085	,000224	-,000526	,000355
	Varianzgleichheit nicht angenommen			-,380	993,848	,704	-,000085	,000224	-,000526	,000355
NDVI	Varianzgleichheit angenommen	1,075	,300	1,332	1022	,183	,00480	,00360	-,00227	,01186
	Varianzgleichheit nicht angenommen			1,332	1008,512	,183	,00480	,00360	-,00227	,01186

C.2. SPSS output tables for the independent samples t-test for each year per sample between the ring-barked and control group.

C.2.1. Year 1

Table C.1.: Unpaired t-test, year 1 - sample 1

Gruppenstatistik[a]

	ring_barked	H	Mittelwert	Standardabweichung	Standardfehler Mittelwert
RENDVI	1	128	,570670	,0290178	,0025648
	2	128	,543693	,0352811	,0031184
NDWI	1	128	,133793	,0065634	,0005801
	2	128	,130302	,0210463	,0018602
PSRI	1	128	-,018672	,0045645	,0004034
	2	128	-,019356	,0055938	,0004944
NDLI	1	128	,051090	,0024519	,0002167
	2	128	,050836	,0019297	,0001706
NDVI	1	128	,862853	,0133744	,0011821
	2	128	,859125	,0115876	,0010242

a. year = 1

Test bei unabhängigen Stichproben[a]

		Levene-Test der Varianzgleichheit		T-Test für die Mittelwertgleichheit						
									95% Konfidenzintervall der Differenz	
		F	Sig.	t	df	Sig. (2-seitig)	Mittelwertdifferenz	Standardfehlerdifferenz	Unterer	Oberer
RENDVI	Varianzgleichheit angenommen	17,365	,000	6,681	254	,000	,0269772	,0040377	,0190256	,0349289
	Varianzgleichheit nicht angenommen			6,681	244,880	,000	,0269772	,0040377	,0190242	,0349303
NDWI	Varianzgleichheit angenommen	270,298	,000	1,792	254	,074	,0034916	,0019486	-,0003459	,0073290
	Varianzgleichheit nicht angenommen			1,792	151,471	,075	,0034916	,0019486	-,0003584	,0073415
PSRI	Varianzgleichheit angenommen	8,472	,004	1,071	254	,285	,0006835	,0006381	-,0005733	,0019402
	Varianzgleichheit nicht angenommen			1,071	244,176	,285	,0006835	,0006381	-,0005735	,0019404
NDLI	Varianzgleichheit angenommen	11,699	,001	,924	254	,356	,0002549	,0002758	-,0002882	,0007980
	Varianzgleichheit nicht angenommen			,924	240,704	,356	,0002549	,0002758	-,0002883	,0007982
NDVI	Varianzgleichheit angenommen	1,890	,170	2,383	254	,018	,0037280	,0015641	,0006477	,0068083
	Varianzgleichheit nicht angenommen			2,383	248,949	,018	,0037280	,0015641	,0006474	,0068086

a. year = 1

Table C.2.: Unpaired t-test, year 1 - sample 2

Gruppenstatistik[a]

	ring_barked	H	Mittelwert	Standardabweichung	Standardfehler Mittelwert
RENDVI	1	128	,567299	,0208201	,0018403
	2	128	,566074	,0326272	,0028839
NDWI	1	128	,132125	,0233053	,0020599
	2	128	,139356	,0150974	,0013344
PSRI	1	128	-,017690	,0034329	,0003034
	2	128	-,020257	,0052609	,0004650
NDLI	1	128	,050357	,0026555	,0002347
	2	128	,050446	,0023774	,0002101
NDVI	1	128	,865160	,0128379	,0011347
	2	128	,863398	,0146330	,0012934

a. year = 1

Test bei unabhängigen Stichproben[a]

		Levene-Test der Varianzgleichheit		T-Test für die Mittelwertgleichheit						
									95% Konfidenzintervall der Differenz	
		F	Sig.	t	df	Sig. (2-seitig)	Mittelwertdifferenz	Standardfehlerdifferenz	Unterer	Oberer
RENDVI	Varianzgleichheit angenommen	15,552	,000	,358	254	,721	,0012244	,0034210	-,0055127	,0079615
	Varianzgleichheit nicht angenommen			,358	215,718	,721	,0012244	,0034210	-,0055185	,0079672
NDWI	Varianzgleichheit angenommen	1,897	,170	-2,946	254	,004	-,0072311	,0024544	-,0120647	-,0023976
	Varianzgleichheit nicht angenommen			-2,946	217,631	,004	-,0072311	,0024544	-,0120685	-,0023937
PSRI	Varianzgleichheit angenommen	22,601	,000	4,622	254	,000	,0025666	,0005552	,0014731	,0036601
	Varianzgleichheit nicht angenommen			4,622	218,554	,000	,0025666	,0005552	,0014723	,0036609
NDLI	Varianzgleichheit angenommen	2,480	,117	-,282	254	,778	-,0000890	,0003150	-,0007094	,0005315
	Varianzgleichheit nicht angenommen			-,282	250,953	,778	-,0000890	,0003150	-,0007094	,0005315
NDVI	Varianzgleichheit angenommen	5,535	,019	1,024	254	,307	,0017613	,0017206	-,0016271	,0051498
	Varianzgleichheit nicht angenommen			1,024	249,770	,307	,0017613	,0017206	-,0016274	,0051500

a. year = 1

Table C.3.: Unpaired t-test, year 1 - sample 3

Gruppenstatistik[a]

	ring_barked	H	Mittelwert	Standardabweichung	Standardfehler Mittelwert
RENDVI	1	128	,548234	,0263588	,0023298
	2	128	,553157	,0342293	,0030255
NDWI	1	128	,129043	,0272929	,0024124
	2	128	,136051	,0160769	,0014210
PSRI	1	128	-,017686	,0041219	,0003643
	2	128	-,019372	,0058589	,0005179
NDLI	1	128	,050139	,0026024	,0002300
	2	128	,050582	,0026682	,0002358
NDVI	1	128	,862902	,0127752	,0011292
	2	128	,864030	,0148646	,0013139

a. year = 1

Test bei unabhängigen Stichproben[a]

		Levene-Test der Varianzgleichheit		T-Test für die Mittelwertgleichheit						
									95% Konfidenzintervall der Differenz	
		F	Sig.	t	df	Sig. (2-seitig)	Mittelwertdifferenz	Standardfehlerdifferenz	Unterer	Oberer
RENDVI	Varianzgleichheit angenommen	13,359	,000	-1,289	254	,199	-,0049229	,0038186	-,0124430	,0025972
	Varianzgleichheit nicht angenommen			-1,289	238,436	,199	-,0049229	,0038186	-,0124453	,0025996
NDWI	Varianzgleichheit angenommen	34,454	,000	-2,503	254	,013	-,0070075	,0027998	-,0125213	-,0014938
	Varianzgleichheit nicht angenommen			-2,503	205,663	,013	-,0070075	,0027998	-,0125275	-,0014875
PSRI	Varianzgleichheit angenommen	29,512	,000	2,663	254	,008	,0016864	,0006332	,0004394	,0029333
	Varianzgleichheit nicht angenommen			2,663	227,981	,008	,0016864	,0006332	,0004387	,0029340
NDLI	Varianzgleichheit angenommen	,000	,989	-1,343	254	,181	-,0004424	,0003294	-,0010912	,0002064
	Varianzgleichheit nicht angenommen			-1,343	253,842	,181	-,0004424	,0003294	-,0010912	,0002064
NDVI	Varianzgleichheit angenommen	11,585	,001	-,651	254	,515	-,0011283	,0017324	-,0045401	,0022834
	Varianzgleichheit nicht angenommen			-,651	248,387	,515	-,0011283	,0017324	-,0045404	,0022838

a. year = 1

Table C.4.: Unpaired t-test, year 1 - sample 4

Gruppenstatistik[a]

	ring_barked	H	Mittelwert	Standardabweichung	Standardfehler Mittelwert
RENDVI	1	128	,560440	,0217668	,0019239
	2	128	,572576	,0442288	,0039093
NDWI	1	128	,129814	,0201518	,0017812
	2	128	,132897	,0170999	,0015114
PSRI	1	128	-,013272	,0043370	,0003833
	2	128	-,016552	,0060169	,0005318
NDLI	1	128	,049066	,0026198	,0002316
	2	128	,049809	,0026645	,0002355
NDVI	1	128	,872333	,0119240	,0010539
	2	128	,868796	,0202418	,0017891

a. year = 1

Test bei unabhängigen Stichproben[a]

		Levene-Test der Varianzgleichheit		T-Test für die Mittelwertgleichheit						
									95% Konfidenzintervall der Differenz	
		F	Sig.	t	df	Sig. (2-seitig)	Mittelwertdifferenz	Standardfehlerdifferenz	Unterer	Oberer
RENDVI	Varianzgleichheit angenommen	52,981	,000	-2,785	254	,006	-,0121363	,0043571	-,0207170	-,0035557
	Varianzgleichheit nicht angenommen			-2,785	185,111	,006	-,0121363	,0043571	-,0207323	-,0035404
NDWI	Varianzgleichheit angenommen	1,234	,268	-1,319	254	,188	-,0030822	,0023360	-,0076826	,0015183
	Varianzgleichheit nicht angenommen			-1,319	247,445	,188	-,0030822	,0023360	-,0076832	,0015188
PSRI	Varianzgleichheit angenommen	27,906	,000	5,004	254	,000	,0032803	,0006556	,0019892	,0045713
	Varianzgleichheit nicht angenommen			5,004	230,918	,000	,0032803	,0006556	,0019886	,0045719
NDLI	Varianzgleichheit angenommen	,508	,477	-2,251	254	,025	-,0007435	,0003303	-,0013939	-,0000930
	Varianzgleichheit nicht angenommen			-2,251	253,927	,025	-,0007435	,0003303	-,0013939	-,0000930
NDVI	Varianzgleichheit angenommen	42,716	,000	1,703	254	,090	,0035368	,0020765	-,0005526	,0076261
	Varianzgleichheit nicht angenommen			1,703	205,668	,090	,0035368	,0020765	-,0005572	,0076307

a. year = 1

C.2.2. Year 2

Table C.5.: Unpaired t-test, year 2 - sample 1

Gruppenstatistik[a]

	ring_barked	H	Mittelwert	Standardabweichung	Standardfehler Mittelwert
RENDVI	1	120	,592057	,0218490	,0019945
	2	120	,591720	,0335519	,0030629
NDWI	1	120	,096671	,0109921	,0010034
	2	120	,099701	,0088511	,0008080
PSRI	1	120	-,012763	,0033913	,0003096
	2	120	-,014981	,0054491	,0004974
NDLI	1	120	,048928	,0024475	,0002234
	2	120	,049786	,0023452	,0002141
NDVI	1	120	,859010	,0165677	,0015124
	2	120	,854294	,0188123	,0017173

a. year = 2

Test bei unabhängigen Stichproben[a]

		Levene-Test der Varianzgleichheit		T-Test für die Mittelwertgleichheit						
									95% Konfidenzintervall der Differenz	
		F	Sig.	t	df	Sig. (2-seitig)	Mittelwertdifferenz	Standardfehlerdifferenz	Unterer	Oberer
RENDVI	Varianzgleichheit angenommen	9,671	,002	,092	238	,927	,0003369	,0036550	-,0068634	,0075373
	Varianzgleichheit nicht angenommen			,092	204,543	,927	,0003369	,0036550	-,0068694	,0075433
NDWI	Varianzgleichheit angenommen	1,309	,254	-2,352	238	,020	-,0030295	,0012883	-,0055675	-,0004916
	Varianzgleichheit nicht angenommen			-2,352	227,643	,020	-,0030295	,0012883	-,0055680	-,0004910
PSRI	Varianzgleichheit angenommen	19,057	,000	3,785	238	,000	,0022179	,0005859	,0010637	,0033722
	Varianzgleichheit nicht angenommen			3,785	199,159	,000	,0022179	,0005859	,0010626	,0033733
NDLI	Varianzgleichheit angenommen	,054	,816	-2,772	238	,006	-,0008578	,0003094	-,0014674	-,0002482
	Varianzgleichheit nicht angenommen			-2,772	237,567	,006	-,0008578	,0003094	-,0014674	-,0002482
NDVI	Varianzgleichheit angenommen	,998	,319	2,061	238	,040	,0047164	,0022884	,0002084	,0092244
	Varianzgleichheit nicht angenommen			2,061	234,259	,040	,0047164	,0022884	,0002080	,0092248

a. year = 2

Table C.6.: Unpaired t-test, year 2 - sample 2

Gruppenstatistik[a]

	ring_barked	H	Mittelwert	Standardabweichung	Standardfehler Mittelwert
RENDVI	1	128	,576282	,0320881	,0028362
	2	128	,578741	,0371325	,0032821
NDWI	1	128	,101729	,0145757	,0012883
	2	128	,103327	,0095121	,0008408
PSRI	1	128	-,014388	,0042973	,0003798
	2	128	-,014536	,0046874	,0004143
NDLI	1	128	,049597	,0023674	,0002092
	2	128	,050247	,0021906	,0001936
NDVI	1	128	,855825	,0167687	,0014822
	2	128	,855348	,0181549	,0016047

a. year = 2

Test bei unabhängigen Stichproben[a]

		Levene-Test der Varianzgleichheit		T-Test für die Mittelwertgleichheit						
									95% Konfidenzintervall der Differenz	
		F	Sig.	t	df	Sig. (2-seitig)	Mittelwertdifferenz	Standardfehlerdifferenz	Unterer	Oberer
RENDVI	Varianzgleichheit angenommen	1,625	,204	-,567	254	,571	-,0024593	,0043378	-,0110019	,0060833
	Varianzgleichheit nicht angenommen			-,567	248,771	,571	-,0024593	,0043378	-,0110027	,0060841
NDWI	Varianzgleichheit angenommen	27,172	,000	-1,039	254	,300	-,0015977	,0015384	-,0046273	,0014320
	Varianzgleichheit nicht angenommen			-1,039	218,567	,300	-,0015977	,0015384	-,0046296	,0014343
PSRI	Varianzgleichheit angenommen	,359	,549	,262	254	,793	,0001474	,0005621	-,0009595	,0012543
	Varianzgleichheit nicht angenommen			,262	252,107	,793	,0001474	,0005621	-,0009595	,0012544
NDLI	Varianzgleichheit angenommen	,504	,478	-2,283	254	,023	-,0006508	,0002851	-,0012122	-,0000893
	Varianzgleichheit nicht angenommen			-2,283	252,486	,023	-,0006508	,0002851	-,0012122	-,0000893
NDVI	Varianzgleichheit angenommen	5,077	,025	,218	254	,828	,0004763	,0021844	-,0038257	,0047782
	Varianzgleichheit nicht angenommen			,218	252,414	,828	,0004763	,0021844	-,0038258	,0047783

a. year = 2

Table C.7.: Unpaired t-test, year 2 - sample 3

Gruppenstatistik[a]

	ring_barked	H	Mittelwert	Standardabweichung	Standardfehler Mittelwert
RENDVI	1	128	,578374	,0226549	,0020024
	2	128	,567974	,0400135	,0035367
NDWI	1	128	,107180	,0078067	,0006900
	2	128	,104124	,0088045	,0007782
PSRI	1	128	-,012431	,0075170	,0006644
	2	128	-,016438	,0053583	,0004736
NDLI	1	128	,049371	,0021746	,0001922
	2	128	,049927	,0024041	,0002125
NDVI	1	128	,859595	,0237102	,0020957
	2	128	,848938	,0182421	,0016124

a. year = 2

Test bei unabhängigen Stichproben[a]

		Levene-Test der Varianzgleichheit		T-Test für die Mittelwertgleichheit						
									95% Konfidenzintervall der Differenz	
		F	Sig.	t	df	Sig. (2-seitig)	Mittelwertdifferenz	Standardfehlerdifferenz	Unterer	Oberer
RENDVI	Varianzgleichheit angenommen	42,118	,000	2,559	254	,011	,0104005	,0040643	,0023966	,0184045
	Varianzgleichheit nicht angenommen			2,559	200,835	,011	,0104005	,0040643	,0023865	,0184146
NDWI	Varianzgleichheit angenommen	8,270	,004	2,938	254	,004	,0030562	,0010401	,0010080	,0051045
	Varianzgleichheit nicht angenommen			2,938	250,411	,004	,0030562	,0010401	,0010078	,0051046
PSRI	Varianzgleichheit angenommen	2,198	,139	4,911	254	,000	,0040068	,0008159	,0024000	,0056137
	Varianzgleichheit nicht angenommen			4,911	229,577	,000	,0040068	,0008159	,0023991	,0056145
NDLI	Varianzgleichheit angenommen	2,841	,093	-1,940	254	,054	-,0005558	,0002865	-,0011200	,0000085
	Varianzgleichheit nicht angenommen			-1,940	251,485	,054	-,0005558	,0002865	-,0011201	,0000085
NDVI	Varianzgleichheit angenommen	,017	,897	4,030	254	,000	,0106572	,0026442	,0054499	,0158646
	Varianzgleichheit nicht angenommen			4,030	238,340	,000	,0106572	,0026442	,0054483	,0158662

a. year = 2

Table C.8.: Unpaired t-test, year 2 - sample 4

Gruppenstatistik[a]

	ring_barked	H	Mittelwert	Standardabweichung	Standardfehler Mittelwert
RENDVI	1	128	,582285	,0263366	,0023279
	2	128	,576525	,0407728	,0036038
NDWI	1	128	,103938	,0121554	,0010744
	2	128	,103252	,0136497	,0012065
PSRI	1	128	-,010335	,0033976	,0003003
	2	128	-,011630	,0035682	,0003154
NDLI	1	128	,049597	,0024707	,0002184
	2	128	,050044	,0020907	,0001848
NDVI	1	128	,866969	,0123229	,0010892
	2	128	,860616	,0176967	,0015642

a. year = 2

Test bei unabhängigen Stichproben[a]

		Levene-Test der Varianzgleichheit		T-Test für die Mittelwertgleichheit						
									95% Konfidenzintervall der Differenz	
		F	Sig.	t	df	Sig. (2-seitig)	Mittelwertdifferenz	Standardfehlerdifferenz	Unterer	Oberer
RENDVI	Varianzgleichheit angenommen	46,861	,000	1,343	254	,181	,0057598	,0042903	-,0026892	,0142089
	Varianzgleichheit nicht angenommen			1,343	217,264	,181	,0057598	,0042903	-,0026961	,0142157
NDWI	Varianzgleichheit angenommen	1,014	,315	,425	254	,671	,0006866	,0016155	-,0024949	,0038682
	Varianzgleichheit nicht angenommen			,425	250,660	,671	,0006866	,0016155	-,0024951	,0038684
PSRI	Varianzgleichheit angenommen	1,090	,298	2,975	254	,003	,0012954	,0004355	,0004378	,0021530
	Varianzgleichheit nicht angenommen			2,975	253,393	,003	,0012954	,0004355	,0004378	,0021530
NDLI	Varianzgleichheit angenommen	4,369	,038	-1,564	254	,119	-,0004474	,0002861	-,0010108	,0001160
	Varianzgleichheit nicht angenommen			-1,564	247,228	,119	-,0004474	,0002861	-,0010109	,0001160
NDVI	Varianzgleichheit angenommen	22,681	,000	3,333	254	,001	,0063535	,0019060	,0025999	,0101072
	Varianzgleichheit nicht angenommen			3,333	226,716	,001	,0063535	,0019060	,0025977	,0101094

a. year = 2

C.2.3. Year 3

Table C.9.: Unpaired t-test, year 3 - sample 1

Gruppenstatistik[a]

	ring_barked	H	Mittelwert	Standardabweichung	Standardfehler Mittelwert
RENDVI	1	128	,546690	,0367648	,0032496
	2	128	,549344	,0208991	,0018472
NDWI	1	128	,051789	,0188167	,0016632
	2	128	,060673	,0133400	,0011791
PSRI	1	128	-,006392	,0027896	,0002466
	2	128	-,007984	,0043492	,0003844
NDLI	1	128	,046563	,0029030	,0002566
	2	128	,045960	,0022934	,0002027
NDVI	1	128	,842064	,0212045	,0018742
	2	128	,838809	,0144932	,0012810

a. year = 3

Test bei unabhängigen Stichproben[a]

		Levene-Test der Varianzgleichheit		T-Test für die Mittelwertgleichheit						
									95% Konfidenzintervall der Differenz	
		F	Sig.	t	df	Sig. (2-seitig)	Mittelwertdifferenz	Standardfehlerdifferenz	Unterer	Oberer
RENDVI	Varianzgleichheit angenommen	24,865	,000	-,710	254	,478	-,0026542	,0037379	-,0100154	,0047071
	Varianzgleichheit nicht angenommen			-,710	201,317	,478	-,0026542	,0037379	-,0100247	,0047163
NDWI	Varianzgleichheit angenommen	22,067	,000	-4,357	254	,000	-,0088836	,0020387	-,0128986	-,0048687
	Varianzgleichheit nicht angenommen			-4,357	228,916	,000	-,0088836	,0020387	-,0129007	-,0048666
PSRI	Varianzgleichheit angenommen	22,030	,000	3,486	254	,001	,0015920	,0004567	,0006926	,0024914
	Varianzgleichheit nicht angenommen			3,486	216,370	,001	,0015920	,0004567	,0006919	,0024922
NDLI	Varianzgleichheit angenommen	4,531	,034	1,845	254	,066	,0006032	,0003270	-,0000408	,0012472
	Varianzgleichheit nicht angenommen			1,845	241,087	,066	,0006032	,0003270	-,0000410	,0012473
NDVI	Varianzgleichheit angenommen	11,116	,001	1,434	254	,153	,0032556	,0022702	-,0012152	,0077264
	Varianzgleichheit nicht angenommen			1,434	224,402	,153	,0032556	,0022702	-,0012180	,0077292

a. year = 3

Table C.10.: Unpaired t-test, year 3 - sample 2

Gruppenstatistik[a]

	ring_barked	H	Mittelwert	Standardabweichung	Standardfehler Mittelwert
RENDVI	1	128	,519298	,0414258	,0036616
	2	128	,521070	,0293847	,0025973
NDWI	1	128	,053416	,0170339	,0015056
	2	128	,059035	,0123850	,0010947
PSRI	1	128	-,008727	,0059088	,0005223
	2	128	-,010516	,0045988	,0004065
NDLI	1	128	,045748	,0016242	,0001436
	2	128	,046570	,0022521	,0001991
NDVI	1	128	,834882	,0177050	,0015649
	2	128	,832570	,0190242	,0016815

a. year = 3

Test bei unabhängigen Stichproben[a]

		Levene-Test der Varianzgleichheit		T-Test für die Mittelwertgleichheit						
									95% Konfidenzintervall der Differenz	
		F	Sig.	t	df	Sig. (2-seitig)	Mittelwertdifferenz	Standardfehlerdifferenz	Unterer	Oberer
RENDVI	Varianzgleichheit angenommen	11,846	,001	-,395	254	,693	-,0017714	,0044892	-,0106122	,0070693
	Varianzgleichheit nicht angenommen			-,395	228,983	,694	-,0017714	,0044892	-,0106168	,0070740
NDWI	Varianzgleichheit angenommen	10,838	,001	-3,018	254	,003	-,0056183	,0018615	-,0092843	-,0019524
	Varianzgleichheit nicht angenommen			-3,018	231,946	,003	-,0056183	,0018615	-,0092859	-,0019507
PSRI	Varianzgleichheit angenommen	9,104	,003	2,703	254	,007	,0017892	,0006618	,0004859	,0030925
	Varianzgleichheit nicht angenommen			2,703	239,557	,007	,0017892	,0006618	,0004855	,0030929
NDLI	Varianzgleichheit angenommen	8,993	,003	-3,352	254	,001	-,0008228	,0002454	-,0013061	-,0003394
	Varianzgleichheit nicht angenommen			-3,352	230,977	,001	-,0008228	,0002454	-,0013063	-,0003392
NDVI	Varianzgleichheit angenommen	,043	,836	1,007	254	,315	,0023123	,0022971	-,0022114	,0068360
	Varianzgleichheit nicht angenommen			1,007	252,699	,315	,0023123	,0022971	-,0022115	,0068362

a. year = 3

Table C.11.: Unpaired t-test, year 3 - sample 3

Gruppenstatistik[a]

	ring_barked	H	Mittelwert	Standardabweichung	Standardfehler Mittelwert
RENDVI	1	128	,504663	,0292126	,0025821
	2	126	,512939	,0336328	,0029963
NDWI	1	128	,057023	,0073374	,0006485
	2	126	,070679	,0135585	,0012079
PSRI	1	128	-,007577	,0030838	,0002726
	2	126	-,008527	,0167404	,0014914
NDLI	1	128	,046387	,0026151	,0002311
	2	126	,047211	,0022564	,0002010
NDVI	1	128	,836078	,0174142	,0015392
	2	126	,834732	,0312003	,0027795

a. year = 3

Test bei unabhängigen Stichproben[a]

		Levene-Test der Varianzgleichheit		T-Test für die Mittelwertgleichheit						
									95% Konfidenzintervall der Differenz	
		F	Sig.	t	df	Sig. (2-seitig)	Mittelwertdifferenz	Standardfehlerdifferenz	Unterer	Oberer
RENDVI	Varianzgleichheit angenommen	2,303	,130	-2,095	252	,037	-,0082757	,0039509	-,0160568	-,0004946
	Varianzgleichheit nicht angenommen			-2,092	246,041	,037	-,0082757	,0039553	-,0160663	-,0004851
NDWI	Varianzgleichheit angenommen	33,872	,000	-10,004	252	,000	-,0136559	,0013651	-,0163443	-,0109676
	Varianzgleichheit nicht angenommen			-9,961	191,773	,000	-,0136559	,0013710	-,0163601	-,0109518
PSRI	Varianzgleichheit angenommen	5,426	,021	,632	252	,528	,0009504	,0015049	-,0020133	,0039142
	Varianzgleichheit nicht angenommen			,627	133,344	,532	,0009504	,0015161	-,0020482	,0039491
NDLI	Varianzgleichheit angenommen	5,037	,026	-2,686	252	,008	-,0008238	,0003067	-,0014278	-,0002199
	Varianzgleichheit nicht angenommen			-2,689	247,761	,008	-,0008238	,0003063	-,0014272	-,0002205
NDVI	Varianzgleichheit angenommen	,052	,820	,426	252	,671	,0013464	,0031641	-,0048851	,0075778
	Varianzgleichheit nicht angenommen			,424	195,338	,672	,0013464	,0031773	-,0049198	,0076125

a. year = 3

Table C.12.: Unpaired t-test, year 3 - sample 4

Gruppenstatistik[a]

	ring_barked	H	Mittelwert	Standardabweichung	Standardfehler Mittelwert
RENDVI	1	128	,477634	,0426471	,0037695
	2	128	,445777	,0787069	,0069568
NDWI	1	128	,045107	,0135428	,0011970
	2	128	,048926	,0271580	,0024004
PSRI	1	128	,013880	,0205130	,0018131
	2	128	,030175	,0557447	,0049272
NDLI	1	128	,045038	,0022957	,0002029
	2	128	,044646	,0040425	,0003573
NDVI	1	128	,803675	,0357606	,0031608
	2	128	,769561	,0859925	,0076007

a. year = 3

Test bei unabhängigen Stichproben[a]

		Levene-Test der Varianzgleichheit		T-Test für die Mittelwertgleichheit						
									95% Konfidenzintervall der Differenz	
		F	Sig.	t	df	Sig. (2-seitig)	Mittelwertdifferenz	Standardfehlerdifferenz	Unterer	Oberer
RENDVI	Varianzgleichheit angenommen	25,918	,000	4,026	254	,000	,0318561	,0079124	,0162739	,0474384
	Varianzgleichheit nicht angenommen			4,026	195,656	,000	,0318561	,0079124	,0162516	,0474607
NDWI	Varianzgleichheit angenommen	20,692	,000	-1,424	254	,156	-,0038196	,0026824	-,0091021	,0014629
	Varianzgleichheit nicht angenommen			-1,424	186,484	,156	-,0038196	,0026824	-,0091113	,0014721
PSRI	Varianzgleichheit angenommen	54,168	,000	-3,104	254	,002	-,0162947	,0052502	-,0266341	-,0059552
	Varianzgleichheit nicht angenommen			-3,104	160,775	,002	-,0162947	,0052502	-,0266629	-,0059264
NDLI	Varianzgleichheit angenommen	35,690	,000	,954	254	,341	,0003921	,0004109	-,0004171	,0012013
	Varianzgleichheit nicht angenommen			,954	201,201	,341	,0003921	,0004109	-,0004181	,0012024
NDVI	Varianzgleichheit angenommen	51,284	,000	4,144	254	,000	,0341139	,0082318	,0179027	,0503251
	Varianzgleichheit nicht angenommen			4,144	169,650	,000	,0341139	,0082318	,0178640	,0503638

a. year = 3

C.2.4. Year 4

Table C.13.: Unpaired t-test, year 4 - sample 1

Gruppenstatistik[a]

	ring_barked	H	Mittelwert	Standardabweichung	Standardfehler Mittelwert
RENDVI	1	128	,541034	,0259864	,0022969
	2	128	,564144	,0313641	,0027722
NDWI	1	128	,046346	,0172137	,0015215
	2	128	,067002	,0162299	,0014345
PSRI	1	128	-,002856	,0029916	,0002644
	2	128	-,003776	,0096818	,0008558
NDLI	1	128	,044263	,0027847	,0002461
	2	128	,046216	,0029385	,0002597
NDVI	1	128	,834348	,0191034	,0016885
	2	128	,845191	,0241063	,0021307

a. year = 4

Test bei unabhängigen Stichproben[a]

		Levene-Test der Varianzgleichheit		T-Test für die Mittelwertgleichheit						
									95% Konfidenzintervall der Differenz	
		F	Sig.	t	df	Sig. (2-seitig)	Mittelwertdifferenz	Standardfehlerdifferenz	Unterer	Oberer
RENDVI	Varianzgleichheit angenommen	4,714	,031	-6,419	254	,000	-,0231103	,0036001	-,0302002	-,0160204
	Varianzgleichheit nicht angenommen			-6,419	245,515	,000	-,0231103	,0036001	-,0302014	-,0160192
NDWI	Varianzgleichheit angenommen	,401	,527	-9,878	254	,000	-,0206555	,0020911	-,0247737	-,0165374
	Varianzgleichheit nicht angenommen			-9,878	253,125	,000	-,0206555	,0020911	-,0247738	-,0165373
PSRI	Varianzgleichheit angenommen	,643	,424	1,026	254	,306	,0009191	,0008957	-,0008448	,0026830
	Varianzgleichheit nicht angenommen			1,026	151,032	,306	,0009191	,0008957	-,0008506	,0026888
NDLI	Varianzgleichheit angenommen	1,138	,287	-5,459	254	,000	-,0019535	,0003578	-,0026582	-,0012488
	Varianzgleichheit nicht angenommen			-5,459	253,269	,000	-,0019535	,0003578	-,0026582	-,0012488
NDVI	Varianzgleichheit angenommen	,668	,414	-3,988	254	,000	-,0108431	,0027186	-,0161970	-,0054891
	Varianzgleichheit nicht angenommen			-3,988	241,396	,000	-,0108431	,0027186	-,0161984	-,0054878

a. year = 4

Table C.14.: Unpaired t-test, year 4 - sample 2

Gruppenstatistik[a]

	ring_barked	H	Mittelwert	Standardabweichung	Standardfehler Mittelwert
RENDVI	1	128	,538172	,0426964	,0037739
	2	128	,552805	,0292821	,0025882
NDWI	1	128	,068214	,0196040	,0017328
	2	128	,075479	,0120527	,0010653
PSRI	1	128	-,006292	,0034118	,0003016
	2	128	-,006110	,0042132	,0003724
NDLI	1	128	,045742	,0029421	,0002601
	2	128	,046029	,0030822	,0002724
NDVI	1	128	,843186	,0191157	,0016896
	2	128	,846543	,0155496	,0013744

a. year = 4

Test bei unabhängigen Stichproben[a]

		Levene-Test der Varianzgleichheit		T-Test für die Mittelwertgleichheit						
									95% Konfidenzintervall der Differenz	
		F	Sig.	t	df	Sig. (2-seitig)	Mittelwertdifferenz	Standardfehlerdifferenz	Unterer	Oberer
RENDVI	Varianzgleichheit angenommen	2,798	,096	-3,198	254	,002	-,0146337	,0045761	-,0236457	-,0056218
	Varianzgleichheit nicht angenommen			-3,198	224,827	,002	-,0146337	,0045761	-,0236513	-,0056162
NDWI	Varianzgleichheit angenommen	78,549	,000	-3,571	254	,000	-,0072645	,0020341	-,0112703	-,0032587
	Varianzgleichheit nicht angenommen			-3,571	211,007	,000	-,0072645	,0020341	-,0112742	-,0032548
PSRI	Varianzgleichheit angenommen	9,760	,002	-,380	254	,704	-,0001823	,0004792	-,0011260	,0007614
	Varianzgleichheit nicht angenommen			-,380	243,478	,704	-,0001823	,0004792	-,0011262	,0007616
NDLI	Varianzgleichheit angenommen	,377	,540	-,762	254	,447	-,0002871	,0003766	-,0010288	,0004546
	Varianzgleichheit nicht angenommen			-,762	253,453	,447	-,0002871	,0003766	-,0010288	,0004546
NDVI	Varianzgleichheit angenommen	2,833	,094	-1,541	254	,124	-,0033571	,0021780	-,0076464	,0009322
	Varianzgleichheit nicht angenommen			-1,541	243,891	,125	-,0033571	,0021780	-,0076472	,0009330

a. year = 4

Table C.15.: Unpaired t-test, year 4 - sample 3

Gruppenstatistik[a]

	ring_barked	H	Mittelwert	Standardabweichung	Standardfehler Mittelwert
RENDVI	1	128	,513893	,0455387	,0040251
	2	128	,532344	,0384813	,0034013
NDWI	1	128	,058184	,0229807	,0020312
	2	128	,075896	,0110072	,0009729
PSRI	1	128	-,003996	,0031788	,0002810
	2	128	-,006355	,0039211	,0003466
NDLI	1	128	,043865	,0034610	,0003059
	2	128	,045570	,0036515	,0003227
NDVI	1	128	,833946	,0239336	,0021154
	2	128	,839280	,0194544	,0017195

a. year = 4

Test bei unabhängigen Stichproben[a]

		Levene-Test der Varianzgleichheit		T-Test für die Mittelwertgleichheit						
									95% Konfidenzintervall der Differenz	
		F	Sig.	t	df	Sig. (2-seitig)	Mittelwertdifferenz	Standardfehlerdifferenz	Unterer	Oberer
RENDVI	Varianzgleichheit angenommen	,058	,810	-3,501	254	,001	-,0184507	,0052697	-,0288287	-,0080727
	Varianzgleichheit nicht angenommen			-3,501	247,123	,001	-,0184507	,0052697	-,0288300	-,0080714
NDWI	Varianzgleichheit angenommen	74,126	,000	-7,864	254	,000	-,0177121	,0022522	-,0221475	-,0132767
	Varianzgleichheit nicht angenommen			-7,864	182,358	,000	-,0177121	,0022522	-,0221559	-,0132684
PSRI	Varianzgleichheit angenommen	5,996	,015	5,289	254	,000	,0023596	,0004462	,0014809	,0032382
	Varianzgleichheit nicht angenommen			5,289	243,580	,000	,0023596	,0004462	,0014808	,0032384
NDLI	Varianzgleichheit angenommen	,243	,623	-3,835	254	,000	-,0017052	,0004447	-,0025810	-,0008295
	Varianzgleichheit nicht angenommen			-3,835	253,275	,000	-,0017052	,0004447	-,0025810	-,0008295
NDVI	Varianzgleichheit angenommen	,370	,544	-1,957	254	,051	-,0053344	,0027262	-,0107031	,0000344
	Varianzgleichheit nicht angenommen			-1,957	243,824	,052	-,0053344	,0027262	-,0107042	,0000354

a. year = 4

Table C.16.: Unpaired t-test, year 4 - sample 4

Gruppenstatistik[a]

	ring_barked	H	Mittelwert	Standardabweichung	Standardfehler Mittelwert
RENDVI	1	128	,501240	,0722259	,0063839
	2	128	,527673	,0422200	,0037318
NDWI	1	128	,057748	,0247663	,0021891
	2	128	,069617	,0132818	,0011740
PSRI	1	128	,025631	,0590380	,0052183
	2	128	,003135	,0139836	,0012360
NDLI	1	128	,045470	,0028134	,0002487
	2	128	,045013	,0025514	,0002255
NDVI	1	128	,808115	,0781963	,0069116
	2	128	,832936	,0257561	,0022765

a. year = 4

Test bei unabhängigen Stichproben[a]

		Levene-Test der Varianzgleichheit		T-Test für die Mittelwertgleichheit						
									95% Konfidenzintervall der Differenz	
		F	Sig.	t	df	Sig. (2-seitig)	Mittelwertdifferenz	Standardfehlerdifferenz	Unterer	Oberer
RENDVI	Varianzgleichheit angenommen	2,605	,108	-3,575	254	,000	-,0264334	,0073946	-,0409960	-,0118708
	Varianzgleichheit nicht angenommen			-3,575	204,718	,000	-,0264334	,0073946	-,0410128	-,0118540
NDWI	Varianzgleichheit angenommen	12,914	,000	-4,778	254	,000	-,0118689	,0024840	-,0167607	-,0069771
	Varianzgleichheit nicht angenommen			-4,778	194,470	,000	-,0118689	,0024840	-,0167679	-,0069699
PSRI	Varianzgleichheit angenommen	38,627	,000	4,195	254	,000	,0224963	,0053627	,0119354	,0330573
	Varianzgleichheit nicht angenommen			4,195	141,205	,000	,0224963	,0053627	,0118949	,0330978
NDLI	Varianzgleichheit angenommen	1,364	,244	1,363	254	,174	,0004576	,0003357	-,0002035	,0011187
	Varianzgleichheit nicht angenommen			1,363	251,611	,174	,0004576	,0003357	-,0002036	,0011187
NDVI	Varianzgleichheit angenommen	29,296	,000	-3,411	254	,001	-,0248211	,0072769	-,0391518	-,0104903
	Varianzgleichheit nicht angenommen			-3,411	154,236	,001	-,0248211	,0072769	-,0391963	-,0104458

a. year = 4

Acknowledgements

For supervision of my thesis I would like to thank Prof. Dr. Jan-Peter Mund (HNE Eberswalde) and Dr. Nicole Pinnel (DLR). Many thanks go to the members of the project VitTree, the BaySF, LWF, DLR and BOKU, who initialized this project and supported me with any data needed for my thesis. Special thanks go the department "Land-surface" of the DLR and the team "Applied Spectroscopy" for supporting me with their expert knowledge concerning spectroscopy and data processing. During the whole time I was part of the team which considerably facilitated writing this thesis. Many thanks go to Markus Immitzer from the BOKU who patiently supported me in writing R scripts and kept motivated although the results were unexpected. For introducing me into needle sampling and especially spectra measurements in the laboratory I would like to thank Kathrin Einzmann and Tim Ng for very-super efficient times. Furthermore, thanks go to Prof. Dr. C. Majunke (HNE Eberswalde) for answering patiently all questions concerning bark-beetle attacks and forest diebacks.

Finally I would like to thank people who supported me individually in different ways: My Family, without whose support it would not have been possible. Paul and Rea for calming me down, Kasia for reading the same text again and again and Anne for drinking lots of coffee with me.

Thanks!